Sci. Technol. Arts Res. J., Oct.– Dec. 2024, 13(4), 89-124
DOI: https://doi.org/10.20372/star.V13.i4.08
ISSN: 2226-7522 (Print) and 2305-3372 (Online)
Science, Technology and Arts Research Journal
Sci. Technol. Arts Res. J., Oct. – Dec. 2024, 13(4), 89-124
Journal Homepage: https://journals.wgu.edu.et
Original Research

In Vitro Antibacterial Activity, Molecular docking and ADMET Analysis of Phytochemicals from the Roots of *Stephania abyssimica*

Diriba Borena[1*], Zelalem Abdissa[1], Girmaye Kenasa[2], Fekadu Gurmessa[2], Tolessa Duguma[3], Desalegn Abebe[1], Negera Abdissa[1]

[1]Department of Chemistry, College of Natural and Computational Sciences, Wollega University, Nekemte, Ethiopia
[2]Department of Biology, College of Natural and Computational Sciences, Wollega University, Nekemte, Ethiopia
[3]Department of Chemistry, College of Natural Sciences, Adama Science and Technology University, Adama, Ethiopia

Abstract

Stephania abyssinica is one of the medicinal plants used in Ethiopia to treat different ailments, such as malaria and rabies. This study aimed to isolate the phytochemical components of the root of Stephania abyssinica and evaluate their in vitro and silico biological activities. 5-methoxydurmillone (1), three Anthraquinone derivatives (2, 3, and 4), lupeol (5), and sterol (6 and 7) were isolated from the plant for the first time by silica gel column chromatography and characterized by NMR (1D and 2D) spectroscopy. The antibacterial activity of the crude extract and the isolated compounds was tested against Staphylococcus aureus, Escherichia coli, and Pseudomonas aeruginosa. In silico molecular docking analyses were performed for isolated compounds 1-7 against target proteins E. coli DNA gyrase B, Pseudomonas quinolone signal A PqsA, and S. aureus pyruvate kinas, which revealed minimal binding energies ranging from -7.3 to -8.6 kcal/mol, -6.7 to -9.2 kcal/mol, and -6.4 to -11.1 kcal/mol, respectively. Isolated compounds' antibacterial activity in vitro and silico is regarded as a lead for antibacterial medications. Moreover, these active phytochemicals support the traditional use of this plant against bacterial infections. Provided that in vivo testing is performed for further validation.

Article Information

Article History:
Received: 13-11-2024
Revised: 06-12-2024
Accepted: 16-12-2024

Keywords:
Antibacterial; Drug-likeness; Molecular Docking; Stephania abyssinica; Phytochemicals

*Corresponding Author:
Diriba Borena

E-mail:
diribaborena@gmail.com

INTRODUCTION

There are roughly 60 species in the broad genus *Stephania*, found throughout Asia and Africa (Yiblet et al., 2022). Researchers have shown a great deal of interest in this genus of plants because of their abundance of medicinal phytochemicals, which include protoberberine, morphine, aporphine, hasubanan, and benzylisoquinoline (Zeng et al.,2017), flavonoids, terpenoids, and glycosides (Birhan et al., 2024), which are of particular pharmacological relevance due to their diverse biological activities. One of the herbs frequently used in

Ethiopian traditional medicine to treat various human ailments is *Stephania abyssinica*. The leaves are commonly used to treat abdominal pain (Birhanu et al., 2015; Giday et al., 2010) and rabies (Suleman & Alemu, 2012). The plant's leaves and roots have also been utilized in treating malaria (Zemene et al., 2021). The decoctions of fresh leaves have been used to treat gastritis (Teklehaymanot & Giday, 2007) and snake bites (Giday et al., 2007). The stems have been used for stomach aches and headaches (Teklehaymanot & Giday, 2007). The roots have also been utilized to treat injuries (Mirutse et al., 2009), tumors/cancer (Abebe, 2016), and stomach aches (Firehun & Nedi, 2023). In contrast, the entire plant has been utilized to cure common colds (Zemene et al., 2021). The diverse range of pharmacological activities attributed to *S. abyssinica* underscores the importance of its secondary metabolites in drug discovery. Identifying and isolating these compounds can pave the way for the development of new drugs to treat bacterial infections, oxidative stress-related diseases, inflammatory conditions, and even cancer (Worku et al., 2024). Further, to our knowledge, the phytochemicals present in different parts of the plants, their benefits, and toxicity will not be established and reported to date.

This study aimed to isolate and identify secondary metabolites from the roots of *S. abyssinica* and evaluate their antibacterial properties through in vitro assays. Additionally, the study assessed the toxicity and drug-likeness of the isolated compounds, complemented by an *in silico* molecular-docking analysis to explore their potential interactions with bacterial targets.

MATERIALS AND METHODS

Procedures for General Experiments

Solvents and analytical and HPLC quality reagents were employed in the compounds' extraction and purification processes. The compounds' purity was examined using analytical Silica gel plates with TLC pre-coating (Polygram SIL G/UV254, Macherey-Nagel & Co.). After being misted with 10% H_2SO_4 and heated on a hot plate, the specks were observed under UV light at between 254 and 365 nm. The 500 MHz spectrometer was used to record the NMR spectra, and TMS was used as an internal reference. Chemical shifts are described using parts per million as the unit of measurement. The Agilent Technologies 1200 series Micromass AC-TOF micromass spectrometer in Tokyo, Japan, was utilized for ESI-MS. Gentamycin, Petri dishes, DMSO, and Whatman filter paper No. 3 were utilized for antibacterial purposes.

Plant materials

The *S. abyssinica* roots were gathered in December 2021 from Oromia Regional State's Horro Guduru Wallaga Zone's Amuru District, 382 kilometers from the capital of Ethiopia, Addis Ababa. Prof. Sileshi Nemomisa, a botanist, recognized the plant material, and the National Herbarium received the voucher specimen (DB 004/2022).

Extraction and isolation

A total of (800 g) of the air-dried root of *S. abyssinica* was extracted with CH_2Cl_2/CH_3OH (1:1) three times for 72 hrs at room temperature with random shaking. After filtering and condensing the extract in a rotary evaporator set at 40 °C, 56 g of brown extract was produced. Following a suspension of 40 g of crude extract using *n-hexane* onto 80 g of silica gel with a 60–120 mesh size, the wet sample was subjected to column chromatography. When *n-hexane* was

used to elute the column that contained an increasing percentage of EtOAC, 120 fractions, each 100 mL, were produced. Mixing and further purifying by Sphadex LH-20 fractions 20–26 eluted with 5% EtOAC in hexane provided Compounds **6** (7.5 mg) and **7** (15.1 mg). Using chromatography with silica gel columns (360 mm in length by 60 mm in internal diameter), fractions 31–38 eluted with 10% ethyl acetate in hexane were mixed and purified to yield compound **2** (21 mg). The three spots that fraction 40–52 (40 mg) showed on TLC were combined and further purified to provide compounds **3** (21 mg) and **4** (13.5 mg). Fractions 71–72 yielded the compounds **5** (18 mg) and **1** (13 mg), which were eluted with 30% EtOAC in hexane and subsequently passed *via* gel filtration and Sephadex LH-20, which was eluted with a 1:1 chloroform/methanol mixture.

Antibacterial activity test

Using the agar disc diffusion method, the antibacterial properties of the crude extract and isolated compounds were assessed (Habtamu & Addisu, 2019). One milliliter of bacterial inoculums that are actively growing (from the logarithmic growth phase) and containing about 107 CFU/mL (colony-forming units) (0.5 McFarland Standard) were equally distributed on the agar media using a cotton swab. In these experiments, three different strains of bacteria were used: one gram-positive (*S. aureus;* ATCC25923) and two gram-negative (*E. coli*; ATCC25922) and *P. aeruginosa* (ATCC27853) bacteria. The bacterial pathogens were spread over the agar plate and kept for six minutes at room temperature so that, before the samples were applied, the surface moisture could be absorbed. Concurrently, sterile round Whatman filter paper No. 3 was used to create discs with a diameter of 6 mm. The discs were aseptically put into the Petri dishes of microbial culture. After being impregnated with solutions, the compound and the crude extract were produced in 10% dimethylsulfoxide at a 100 µg/mL concentration. After allowing the applied materials to permeate into the agar for 30 minutes, the mixture was incubated for twenty-four hours at 35°C. Gentamycin (10 µg/disc) was used as the positive control, while 10% DMSO was the negative control to ensure that the solvent did not interfere with bacterial growth. The activities of the crude extracts and isolated compounds were compared against these controls to validate the reliability and effectiveness of the assay. Every test was run in triplicate, and a Vernier caliper was used to measure the inhibition region starting from each disc's edge.

In silico Analysis of the Isolated Compounds

Molecular docking analysis was used to assess the compounds' binding affinities and interactions with the target proteins, which included *S. aureus* pyruvate kinase (PDB ID: 3TO7), *Pseudomonas quinolone signal A*, PqsA (PDB ID: 5OE4), and *E. coli* DNA gyrase B (PDB ID: 7P2M). The proteins were downloaded from the Protein Data Bank (Saur et al., 2021). AutoDock Vina 4.2.6 was used to simulate the protein assembly using the ligand with less energy as input, and the protein was prepared using the standard protocol (Srivastava et al., 2024). It involved eliminating certain water molecules and cofactors, as well as the co-crystallized ligand. The results of the docking computation include hydrogen bond lengths, binding energy (kcal/mol), and an illustration of potential docking placements. Therefore, the isolated compounds' 2D structures were examined using ChemDraw

16.0. ChemBio3D was used to reduce each molecule's energy. Each ligand had nine conformers considered, and the conformer with the greatest docking score was determined to have the lowest binding energy and shown in both 2D and 3D models. The interaction mechanism between every single isolated compound was examined against Gentamycin, an antibacterial drug that served as a comparison positive control in the simulations.

Pharmacokinetic and Toxicity Study of the Isolated Compounds

The PubChem database provided the isolated compounds line-entry systems for simplified molecular-input (SMILESs) that are considered canonical ChemDraw 22.0 was used to sketch and store compounds without SMILES as mol files. To evaluate their physicochemical parameters and drug-likeness (Lipinski rule), they were converted into a SMILES file using the Discovery Studio 12.1 software and uploaded to the SwissADME online platform (Daina et al., 2017). To calculate toxicity endpoints, organ toxicity, and oral acute toxicity. The web-based Pro Tox 3.0 tools received the test chemicals' SMILES files. The results of the isolated compounds were contrasted with those of Gentamycin, and data were also produced for comparison.

Data analysis

Each experiment was run in triplicate. The inhibitory zone data were loaded into SPSS version 20.0, and Tukey's B was used to compare the means of the performances at $\alpha = 0.05$.

RESULTS AND DISCUSSION

Characterization of isolated compounds

Seven compounds **1**–**7** were obtained by chromatographic fractionation and separation of the *S. abyssinica* roots (Figure 1). NMR spectroscopy (1D and 2D) and ESI-MS spectrometry were used to determine the structures of the isolated compounds. The data were compared with published literature to confirm the structure of the isolated compounds. Notably, these compounds have not been previously reported in this plant species.

Compound **1** was identified as a white solid with a melting point of 142-143 °C and a chemical formula of $C_{23}H_{20}O_7$, confirmed by ESI-MS (m/z = 431 $[M+Na]^+$) Appendix 7. The ^{1}H-NMR (500 MHz, $CDCl_3$) spectra, (Table 1 and Appendix 1) revealed the following key features: three doublet protons at δ_H 7.10 (d, J = 1.7 Hz), 6.80 (d, J = 7.8 Hz), and 6.79 (d, J = 10.0 Hz); two methoxyl groups at δ_H 3.92 (s, 3H) and 3.98 (s, 3H); two methyl groups at δ_H 1.57 (s, 6H); a doublet of doublet proton at δ_H 6.96 (dd, J = 8.0, 1.7 Hz); a methine proton at δH 7.83 (s, 1H); and a sp2 system with a doublet proton at δ_H 5.71 (d, J = 10.1 Hz). The ^{13}C-NMR (125 MHZ, $CDCl_3$) spectra, (Table 1 and Appendix 2) revealed 23 carbons, including a carbonyl carbon at δ_C 175.2, an olefinic quaternary carbon at δ_C 125.7, three quaternary aromatic carbons at δ_C 125.7, 113.1, and 106.8, and three methine carbons in the aromatic region at δ_C 125.5, 110.0, and 108.3. Additionally, six oxygenated aromatic carbons were observed at δ_C 140.0, 147.6, 147.7, 149.2, 151.2, and 153.1. Other notable carbons include two methoxy carbons at δ_C 62.2 and 61.5, one methylenedioxy carbon at δ_C 101.1, two olefinic methine carbons at δ_C 129.2 and 115.0, two methyl carbons at δ_C 28.1, and one oxygenated quaternary aliphatic carbon at δ_C 76.7. The methoxy groups at δ_C 62.2 and 61.4, along with

the carbonyl and aromatic carbons. Based on the COSY, HMBC and HSQC shown in Appendix 3-6, the identity of the compounds is 5-methoxydurmillone, previously isolated from Millettia ferruginea (Endale et al., 2016).

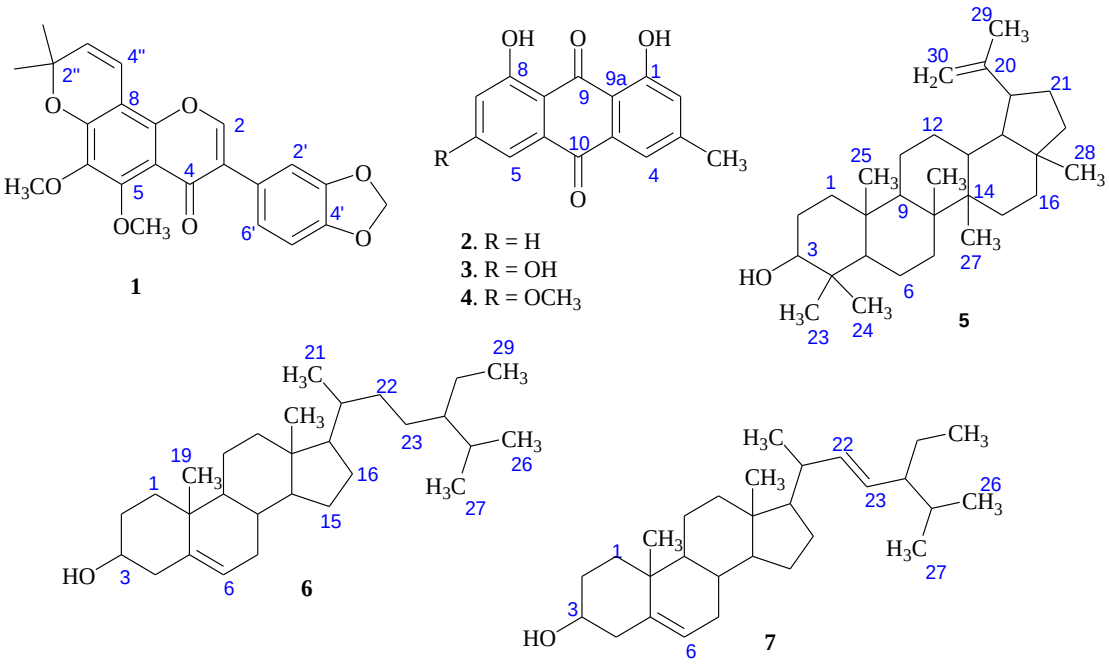

Figure 1: *Chemical structures of the compounds isolated from the roots of S. abyssinica.*

Compounds **2-4** were isolated as yellow solids. The ^{1}H and ^{13}C NMR and spectral data (Table 1 and Appendix 8-11) revealed structural similarities among these compounds. They share the same anthraquinone skeleton, as evidenced by the two downfield shifts that are extremely proton signals around δ_H 12.10 and 11.98 (since chelated hydroxyl protons are involved in hydrogen bonding with a peri-carbonyl group). The compounds' possession of the 1,8-dihydroxyanthraquinone moiety was demonstrated by the two downfield shifted carbonyl signals around δ_C 192.4 and 181.8. Two meta-coupled aromatic protons of H-2 and H-4 are present with the biogenetically expected aromatic C-3 of the di-substituted ring that contains methyl, which is also common for the three compounds. The only noticeable difference is in ring C, where the three mutually coupled aromatic protons for H-5, H-6, and H-7, respectively, in compound **2** and two upfield-shifted *meta*-coupled aromatic protons for H-5 and H-7 in compounds **3** and **4** were observed. In addition, a signal at δ_H 4.11 (δ_C 56.1) for a methoxyl group was also observed in compound **4**. This indicated that C-5 was substituted with hydroxyl and methoxyl groups in **3** and **4**, respectively. Based on a thorough investigation of COSY, HSQC, and HMBCspectrum data (Appendix 12- 19) and comparison with the literature report, the structures of compounds **2**, **3,** and **4** showed that they were chrysophanol. (Tadesse et al., 2022), emodin (Shifa et al., 2021), and physcion respectively. The isolation of these chemicals from this plant species has not been reported before. However, these compounds usually co-occur and are widely distributed in many plant families of *Rhubarb* (Duval et al., 2016).

Table 1

^{1}H-NMR (500 MHz) and ^{13}C-NMR (125 MHz) spectroscopic data of compound 1-4, δ (ppm), in $CDCl_3$

	1		2		3		4	
C/H	δ_H (m, *J* in Hz)	δ_C	δ_H (m, *J* in Hz)	δ_C	δ_H (m, *J* in Hz)	δ_C	δ_H (m, *J* in Hz)	δ_C
1	-	-		162.3		161.8		161.3
2	7.83 (s)	150.3	7.08 (dd, *J* = 1.8, 0.9)	124.5	7.12 (s)	124.5	7.33 (d, *J* = 1.0)	123.9
3	-	125.7	-	149.3	-	148.6		148.2
4	-	175.1	7.63 (d, *J* = 0.8)	119.9	7.43 (d, *J* = 1.5)	120.9	7.69 (d, *J* = 1.0)	120.3
4a	-	106.8		113.6		113.8		113.2
5	-	150.3	7.68 (d, *J* = 7.6)	136.9	7.07 (d,*J* = 2.4)	109.2	7.36 (d, *J* = 2.6)	109.7
6	-	140.0	7.80 (dd, *J* = 7.5, 1.2)	124.3		166.0	-	165.9
7	-	149.1	7.29 (d, *J* = 8.4)	121.1	6.56 (d, *J* = 2.4)	108.3	7.01 (d, *J* = 2.5)	107.3
8	-	113.1	-	162.6	-	164.9	-	164.2
8a	-	153.0	-	115.8	-	109.3	-	106.4
9	-	-	-	192.4	-	190.1	-	189.7
9a	-	-	-	133.2	-	133.2	-	134.7
10	-	-	-	181.8	-	181.7	-	180.9
10a	-	-	-	133.5	-	135.4	-	132.7
3-CH_3	-	-	2.47 (s)	22.2	2.39 (s)	21.9	2.59 (s)	21.2
6-OCH_3	-	61.5		-	-	-	4.11 (s)	56.1
1-OH	-	-	12.10 (s)	-	12.04 (s)	-	12.01 (s)	-
8-OH	-	-	11.98 (s)	-	19.97 (s)	-	12.13 (s)	-
1'	-	125.7	-	-	-	-	-	-
2'	7.10 (d, *J* = 1.7)	110.0	-	-	-	-	-	-
3'	-	147.6	-	-	-	-	-	-
4'	-	147.6	-	-	-	-	-	-
5'	6.80 (d, J= 7.8)	108.3	-	-	-	-	-	-
6'	6.96 (dd, *J* = 8.0, 1.7)	122.5	-	-	-	-	-	-
2''	-	76.7	-	-	-	-	-	-
3''	5.71 (d, *J* = 10.1)	115.0	-	-	-	-	-	-
4''	6.79 (d, *J* = 10.0)	129.2	-	-	-	-	-	-
2''-Me_2	1.57 (s)	28.1	-	-	-	-	-	-
O-CH_2-O	6.00 (s)	101.1	-	-	-	-	-	-
5-OMe	3.98 (s)	62.2	-	-	-	-	-	-
6 –Ome	3.92 (s)	61.4		-	-	-	-	-

Compound **5** was identified as a white solid with a melting point at 215 and 216 °C. Proton signals at δ_H 0.77 (s, 3H), 0.79 (m, 3H), 0.83 (m, 3H), 0.94 (s, 3H), 0.96 (m, 3H), 1.05 (s, 3H), and 1.60 (m, 3H) were detected in the 1H-NMR (500 MHz, CDCl3) spectrum (Appendix 20). These signals correspond to methyl groups at C-24, C-28, C-25, C-27, C-23, C-26, and C-30. In addition, it displayed two non-equivalent (germinal) olefinic protons at δH 4.58 and 4.70, which represent the exocyclic double bond, and a pair of doublets for the oxymethine proton at H-3 at δH 3.20. The well-resolved 30 carbon signals in the 13C and 2D NMR spectrum data (125 MHz, CDCl3) spectrum (Appendix 21) included six quaternary, six methine, seven methyl, and eleven methylene carbons. lupane triterpenoid was confirmed by the exocyclic double bond carbons that were seen at δC 150.9 and 109.3 of C-20 and C-29.

Compound 5 was identified as lupeol based on COSY and HMBC spectrum data (Appendix 22-23) and the previously mentioned spectrum analysis and contrast with data published in the literature (Shwe et al., 2019).etected in the ^{1}H-NMR (500 MHz, $CDCl_3$) spectrum (Appendix 20). These signals correspond to methyl groups at C-24, C-28, C-25, C-27, C-23, C-26, and C-30. In addition, it displayed two non-equivalent (germinal) olefinic protons at δ_H 4.58 and 4.70, which represent the exocyclic double bond, and a pair of doublets for the oxymethine proton at H-3 at δ_H 3.20. The well-resolved 30 carbon signals in the ^{13}C and 2D NMR spectrum data (125 MHz, $CDCl_3$) spectrum (Appendix 21) included six quaternary, six methine, seven methyl, and eleven methylene carbons. lupane triterpenoid was confirmed by the exocyclic double bond carbons that were seen at δ_C 150.9 and 109.3 of C-20 and C-29. Compound **5** was identified as lupeol based on COSY and HMBC spectrum data (Appendix 22-23) and the previously mentioned spectrum analysis and contrast with data published in the literature (Shwe et al., 2019).Compound **6** was a white crystalline solid with m.p. of 134–135 ^{o}C. The proton signals at δ_H 3.55 (dd, J = 10.8, 4.7 Hz) integrated for 1H were seen in the ^{1}H- NMR (500 MHz, CDCl3) spectrum (Appendix 24), indicating a hydroxymethine proton of H-3. The steroidal skeleton olefinic protons of H-6 are often represented as a triplet peak at δ_H 5.37 (t, J = 6.4 Hz, 1H). The methyl proton represents H-18 and H-19 signals at δ_H 0.93 (s, 3H) and 0.58 (s, 3H). There were 29 carbon signals in the ^{13}C-NMR (125 MHz, $CDCl_3$) spectra in Appendix 25, with three quaternary, eleven methine, nine methylene, and six methyl groups. The olefinic carbons at C-5 and C-6 are represented by the identifiable signals at δ_C140.7 and 121.7, respectively. These spectroscopic findings and the data presented in the literature led to the conclusion that compound 6 structure was β-sitosterol. (Uttu et al., 2023).Compound **7** White crystalline solid with a melting point of 174–176 ^{o}C. The ^{1}H and ^{13}C NMR spectra in Appendix 26-27 exhibited similar spectral features as compound **6**, including the steroidal nucleus. The only noticeable difference is the presence of olefinic protons for H-22 (δ_H 5.17) and H-23 (δ_H 4.98) in compound **7**, which has been missed in compound **6**. This is further supported by the ^{13}C NMR(125 MHz, $CDCl_3$) spectrum, which indicates the olefinic carbons C-22 (δ_C138.3) and C-23 (δ_C 129.2) in compound **7**.

Therefore, the Compound 7 structure was determined to be stigmasterol (Alex et al., 2024). Compounds 6 and 7 have likely been

co-isolated in various plants (Ayele et al., 2022; Erwin et al., 2020).

Antibacterial activity

The disc diffusion method was used to assess the antibacterial activity of the crude extract and the identified compounds against strains of *S. aureus*, *E. coli*, and *P. aeruginosa*. Both gram-positive and gram-negative bacterial strains were susceptible to the crude extract's actions. When applied to *S. aureus*, the crude extract (10µg/mL) produced a maximal inhibitory zone of 18.40 mm in diameter, which was comparable to the standard gentamycin (20.03 ± 0.01 mm) at $p<0.05$. Using the same solvent and bacterial strains, this result is better than the one reported before for a crude extract from Hydnorajohannis roots (Degfie et al., 2022). Similar to the reference antibiotics, the crude extract exhibited strong antagonistic effects against the tested bacterial strains, which did not differ significantly from one another at $p<0.05$.

Table 2

The diameter (mm) of the bacterial growth inhibition zone of crude extract and isolated compounds (1–7) (100 µg/mL each) using the agar disc diffusion method.

Test samples	Tested micro-organism		
	S. aureus	*E.coli*	*P. aeruginosa*
1	12.50 ± 0.07^{b}	12.50 ± 0.03^{ab}	8.50 ± 0.01^{b}
2	9.50 ± 0.21^{b}	9.10 ± 0.04^{b}	9.50 ± 0.03^{b}
3	11.50 ± 0.03^{ab}	12.50 ± 0.03^{ab}	9.00 ± 0.22^{b}
4	10.50 ± 0.13^{b}	9.10 ± 0.15^{b}	8.01 ± 0.12^{b}
5	7.00 ± 0.24^{a}	7.01 ± 0.16^{bc}	7.50 ± 0.02^{bc}
6	7.50 ± 0.22^{bc}	8.10 ± 0.10^{b}	7.10 ± 0.21^{bc}
7	8.30 ± 0.11^{b}	10.50 ± 0.10^{b}	7.30 ± 0.02^{bc}
Crude extract	18.40 ± 0.24^{a}	16.02 ± 0.08^{ab}	17.04 ± 0.10^{ab}
DMSO	-	-	-
Gentamycin	20.03 ± 0.01^{a}	18.02 ± 0.02^{a}	21.03 ± 0.04^{a}

Key: *not active; DMSO, dimethylsulfoxide. Results are in mean ± SD of triplicate experiments, and different superscript letters in each row and column indicate that the means are significantly different, and the similar superscript letters indicate that they are comparable with each other at $p < 0.05$.*

The maximum zone of inhibitions for the isolated compounds was 12.50 mm by compound **1** against *S. aureus and E. coli* and compound 3, which was not significantly smaller than the reference antibiotics at $p<0.05$ (Table 2). In general, the compounds showed equivalent antibacterial properties against the tested bacterial strains except compound **5**, in which the antibacterial activity was not detected for *S. aureus* and *E. coli*. In addition, the antibacterial activities of the crude extract and isolated compound against at $p<0.05$, the investigated bacterial strains did not differ significantly.

Molecular docking studies of the Isolated compounds.

The target proteins *Pseudomonas quinolone signal* A, PqsA (PDB ID: 5OE4), *E. coli* DNA gyrase B (PDB ID: 7P2M), and *S. aureus* pyruvate kinase (PDB ID: 3TO7) were the targets of a molecular docking study to assess the binding affinities and interactions of isolated compounds 1–7. The residual interaction, H-bonding, and binding affinity of each isolated chemical are listed in Tables 3-5. The docked compounds 1–7 had minimum binding energies ranging from -7.6 to -9.2 kcal/mol, -7.3 to -8.6 kcal/mol, and -6.4 to -11.1 kcal/mol, respectively. Lower docking score values indicate that the isolated compounds and the protein target interact well. Compounds **1**–**7** showed greater binding affinity against *Pseudomonas* quinolone signal A (PqsA) compared to the standard drug Gentamycin. Compounds **5**, **6**, and **7** did not interact with the amino acid residue, while compounds **1-4** showed H-bonding interaction with Gly-279 similar to gentamycin hydrogen, as indicated in Figure 2 and Table 3

.

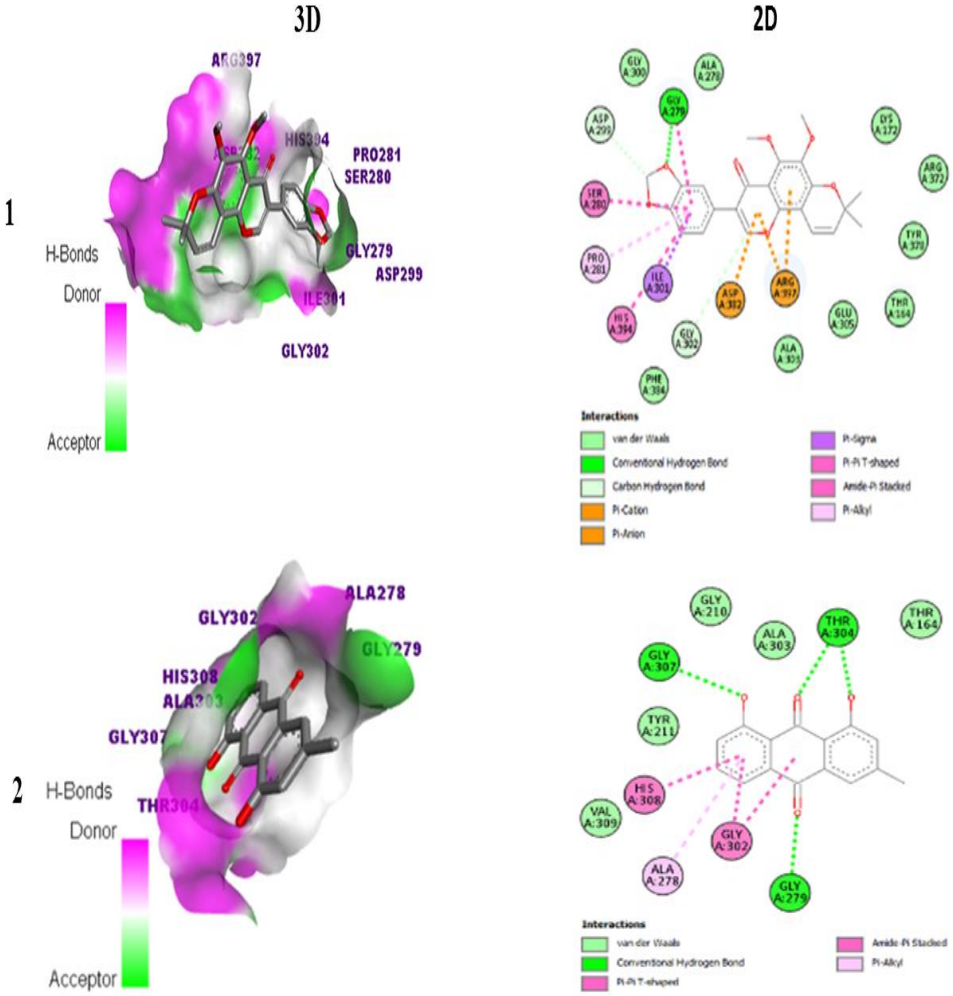

3

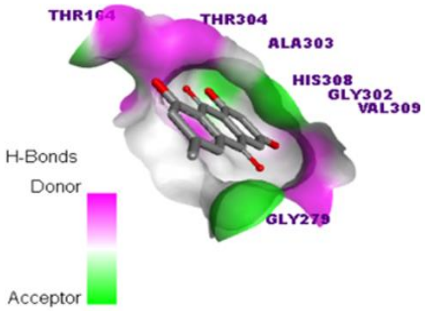
THR164
THR304
ALA303
HIS308
GLY302
VAL309
GLY279
H-Bonds
Donor
Acceptor

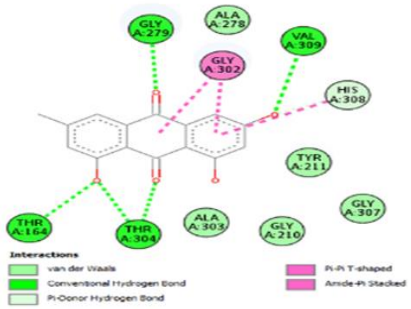
GLY A:279
ALA A:278
VAL A:309
GLY A:302
HIS A:308
TYR A:211
GLY A:307
THR A:164
THR A:304
ALA A:303
GLY A:210
Interactions
van der Waals
Conventional Hydrogen Bond
Pi-Donor Hydrogen Bond
Pi-Pi T-shaped
Amide-Pi Stacked

4

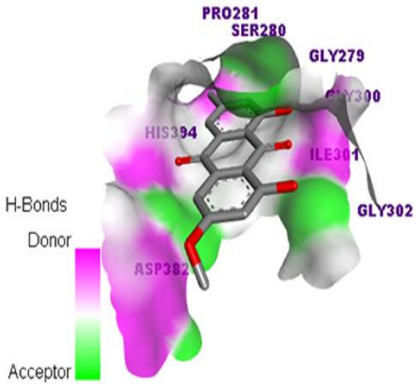
PRO281
SER280
GLY279
HIS394
ILE301
GLY302
ASP382
H-Bonds
Donor
Acceptor

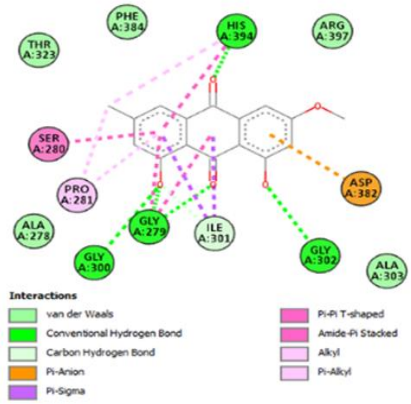
PHE A:384
HIS A:394
ARG A:397
THR A:323
SER A:280
PRO A:281
ASP A:382
ALA A:278
GLY A:279
ILE A:301
GLY A:300
GLY A:302
ALA A:303
Interactions
van der Waals
Conventional Hydrogen Bond
Carbon Hydrogen Bond
Pi-Anion
Pi-Sigma
Pi-Pi T-shaped
Amide-Pi Stacked
Alkyl
Pi-Alkyl

5

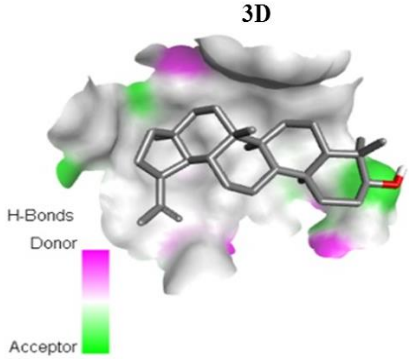
3D
H-Bonds
Donor
Acceptor

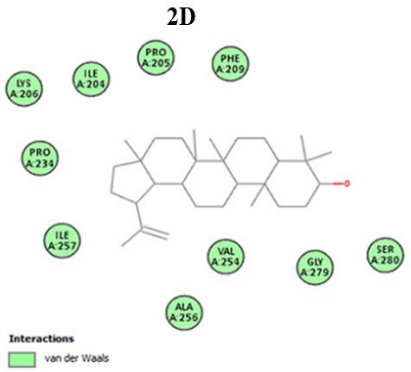
2D
PRO A:205
PHE A:209
LYS A:206
ILE A:204
PRO A:234
ILE A:257
VAL A:254
GLY A:279
SER A:280
ALA A:256
Interactions
van der Waals

6

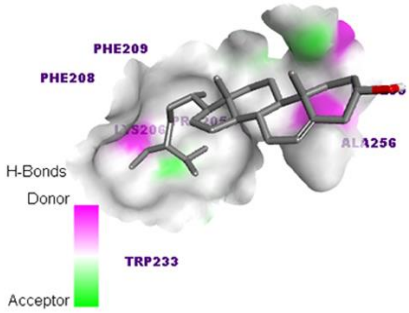
PHE209
PHE208
ALA256
H-Bonds
Donor
TRP233
Acceptor

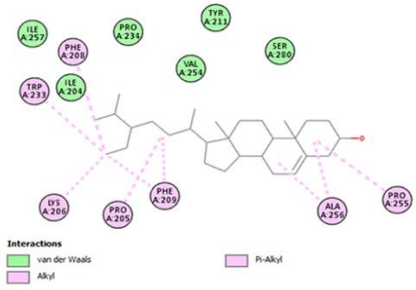
ILE A:257
PRO A:234
TYR A:211
PHE A:208
SER A:280
VAL A:254
TRP A:233
ILE A:204
LYS A:206
PRO A:205
PHE A:209
ALA A:256
PRO A:255
Interactions
van der Waals
Alkyl
Pi-Alkyl

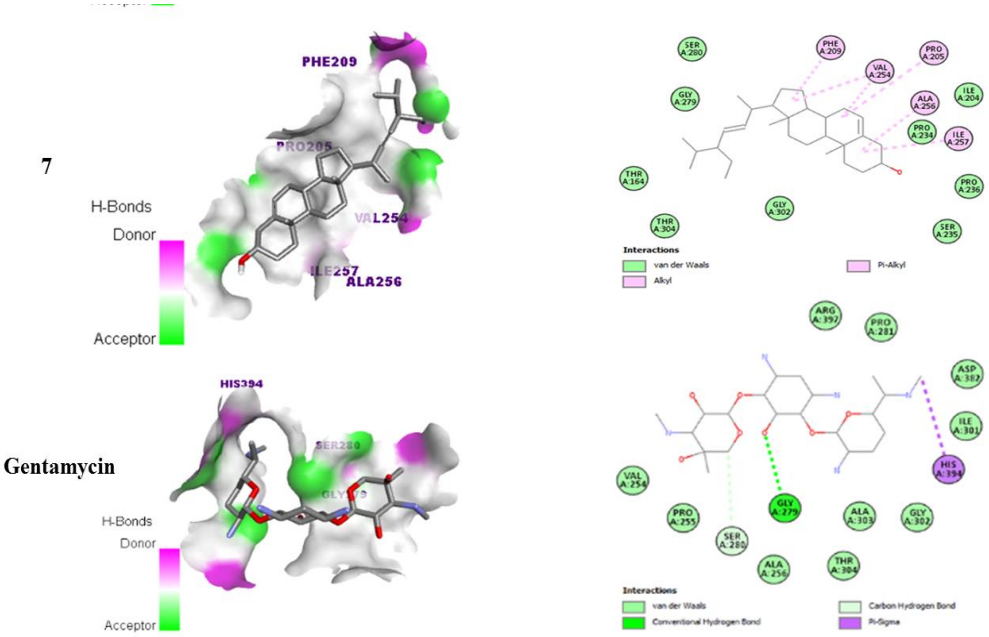

Figure 2. *The 3D and 2D modes of interactions of isolated compounds and Gentamycin against Pqs*

Table 3

Molecular docking results of isolated compounds and Gentamycin against Pseudomonas quinolone signal A (PqsA)

Ligand	Binding	H –bonding	Hydrophobic and Electrostatic	Van der Waals
1	-8.3	Gly-279	Carbon hydrogen bond: Gly-302, Asp-299; Pi-cation and Pi-anion: Asp-382, Arg-397, Arg-397; Pi-sigma: Ile-301; Pi-Pi T shaped and Amide pi stacked: His-394, Ser-280, Gly-279; Pi-alkyl: Pro-281	Phe-384, Ala-303, Glu-305, Thr-164, Tyr-378, Arg-372, Lys172, Ala-278, Gly-300
2	-9.2	Gly-279, Gly-307, Tyr-304	T-shaped and Amide Pi : His-308, Gly-3022, Gly-302; Pi-alkyl: Ala-278	Val-309, Tyr-211, Gly-210, Ala-303, Thr-164
3	-9.0	Thr-164, Thr-304, Thr-304, Val-309, Gly-279	Pi donor hydrogen bond: Ala-303, His-308; Pi-pi T shaped and Amide pi stacked: Gly-302, Gly-302, His	Ala-303, Gly-210, Gly-307, Thr-211, Ala-208
4	-8.0	Gly-300, Gly-279, Gly-279, Gly-302, His-394	Carbon hydrogen bond: Ile-301; Pi-anion: Asp-382; Pi -sigma: Ile-301, Ile-301; Pi -T shaped and Amide pi stacked: Ser-280, Gly-279, Gly-279, His-394; Alkyl and Pi - alkyl: Pro-281, Pro-281, His-394	Ala-278, Thr-323, Phe-384, Arg-397, Ala=303
5	-7.6	-	-	Phe-209, Pro-234, Ile-204,Pro-205, Lys-206 , Ile-257, Ala-256, Ser-280V, Gly-279
6	-6.7	-	Alkyl and Pi -alkyl: Phe-208, Trp-233, Lys-206, Pro-205, Phe-209, Phe-209, Ala-256, Pro255	Ile-257, Ile-204, Pro-234, Val-254, Tyr-211, Ser-250
7	-7.3	-	Alkyl and Pi-alkyl: Phe-209, Val-254, Val-254, Pro-205, Ala-256, Ile-257	Ser-280, Gly-279, Thr-164, Thr-304, Gly-302, Ser-235, Pro-236, Pro-234, Ile-204
Gentamycin	-5.8	Gly-279	Carbon hydrogen bond: Ser-280; Pi-sigma: His-394	Val-254, Pro-255, Ala-256, Thr-304, Ala-303, Gly-302, Ile-301, Asp=382, Pro-281, Arg-397

While compound **2** interacted through three Arg-136, Arg-76, and Gly-77, compounds **1**, **3**, **4**, and **7** can interact with hydrogen via Arg-76, Asn-46, Arg-76, and Asp-73, respectively. Compounds **5** and **6** did not interact with the amino acid residues of *E. coli* DNA gyrase B, as shown in Table 4 and Figure 3, which display the two- and three-dimensional binding interactions of compounds **1**–**7** and gentamycin against *E. coli* DNA gyrase B (PDB ID: 7P2M).

Table 4

Gentamycin and isolated compounds' molecular docking results against E. coli DNA Gyrase B.

Ligand	Binding	H-bonding	Hydrophobic and Electrostatic	Van der Waals
1	-8.6	Arg-76	Carbon hydrogen bond: Gly-77, Asn-46; Pi-alkyl: Val-120, Ile-94, Ile-94, Ile-78, Ile-78, Ile-78	Val-43, Ala-47,Val-71 , Thr-165, Asp-73, Glu-50, Pro-79, Asp-73,
2	-8.2	Arg-136, Arg-76, Arg-76, Gly-77	Pi-cation and pi-anion: Glu-50, Glu-50, Arg-76; Amide pi-stacked: Asn-46; Alkyl and pi-alkyl: Pro-79, pro-79, Ile-78, Ile-78, Ile-78	Ile-94, , Thr-165, Gly-75 ,Val-167
3	-8.6	Asn-46	Pi-anion: Glu-50; Pi-sigma: Ile-78; Amide pi stacked: Gly-77, Gly-77; Alkyl and pi alkyl: Val-167, Val-43, Ile-78, Ile-78	Val-120, Thr-165,Ile-94, Pro-79, Arg-136, Arg-76, Asp-73
4	-8.2	Arg-76	Pi-sigma: Thr-165, Asn-46; Alkyl and pi alkyl: Val-71, Val-43, Ala-47, Ile-78, Ile-78	Val-167, Val-120, Ile-94, Glu-50, Asp-73
5	-7.3	-	-	,Ala-90, Pro-79, His-83,Ile-94, Ile-78, Thr-165, Gly-77, Arg-76, Glu-50, Asn-46, Asp-49
6	-8.0	-	Pi-sigma: His-83; Alkyl and Pi-alkyl: His-83, Val-93, Ala-90, Ala-90, Ala-90, Ile-94, Ile-94, Pro-79, Pro-79, Ile-78, Ile-78	Gly-77,Arg-76, Asn-46, Glu-50Thr-165, Asp-73, Ala-47, Val-43
7	-8.3	Asp-73	Pi-sigma: His-83; Alkyl and Pi-alkyl: Ile-94, Val-93, His-83, Ala-90, Ala-90; Pro-79, Pro-79, Ile-78, Ile-78	Arg-76, Asn-46, Ala-47, Gly-77, Glu-50, Thr-165
Gentamycin	-7.7	Gly-77	Carbon hydrogen bond: Val-97, Ile-94; Alkyl: Ile-78	,Ser-121, Gly-119, Thr-165, Pro-79, Arg-76, Leu-98Glu-50, Asp-73, Val-43, Val-167, Asn-46 Val-120

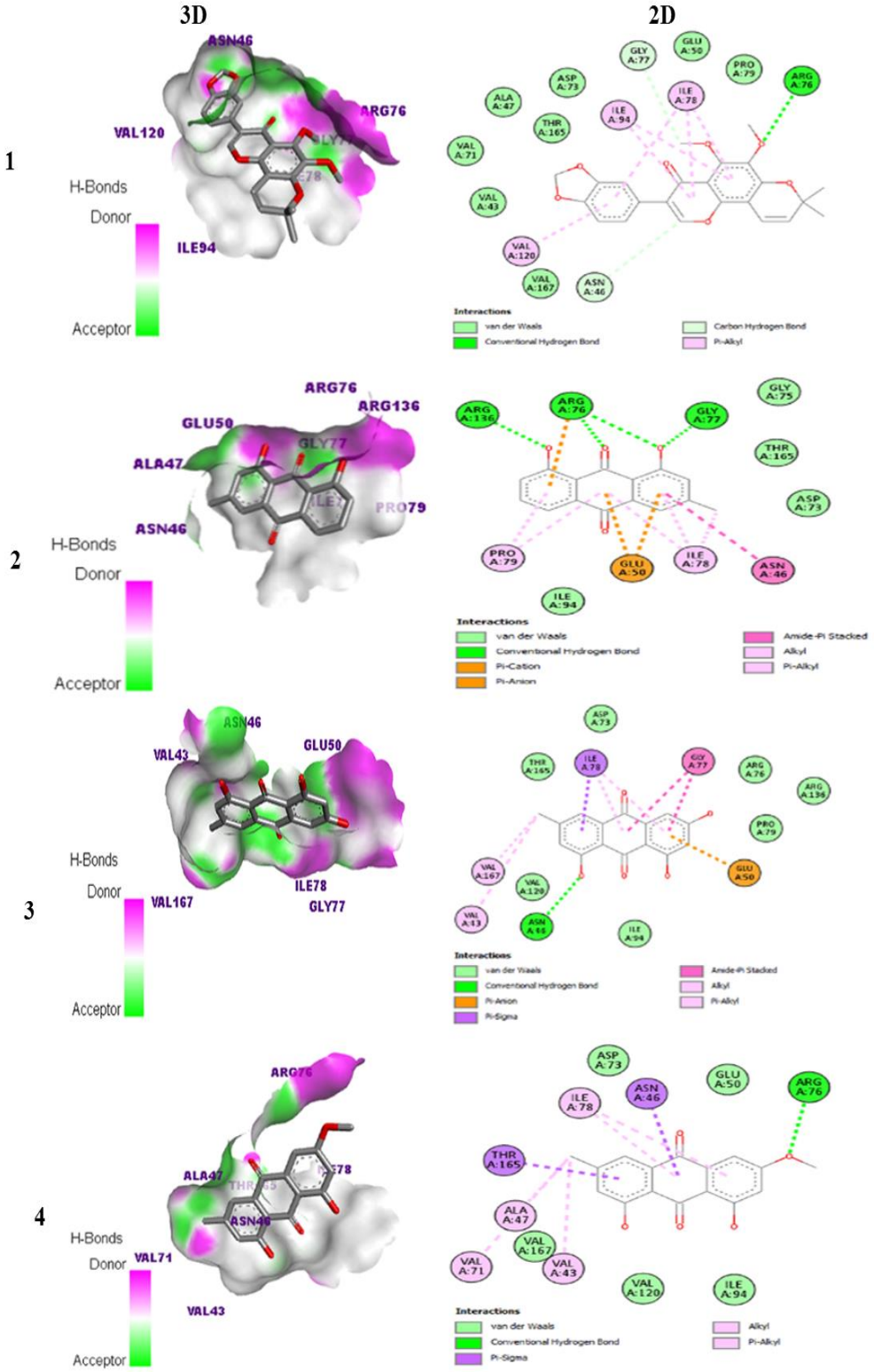
3D
2D
1
ASN46
ARG76
VAL120
ILE94
H-Bonds
Donor
Acceptor
Interactions
van der Waals
Conventional Hydrogen Bond
Carbon Hydrogen Bond
Pi-Alkyl
2
ARG76
ARG136
GLU50
GLY77
ALA47
ASN46
PRO79
Amide-Pi Stacked
Alkyl
Pi-Cation
Pi-Anion
3
ASN46
VAL43
GLU50
ILE78
GLY77
VAL167
Pi-Sigma
4
ARG76
ALA47
ASN46
VAL71
VAL43

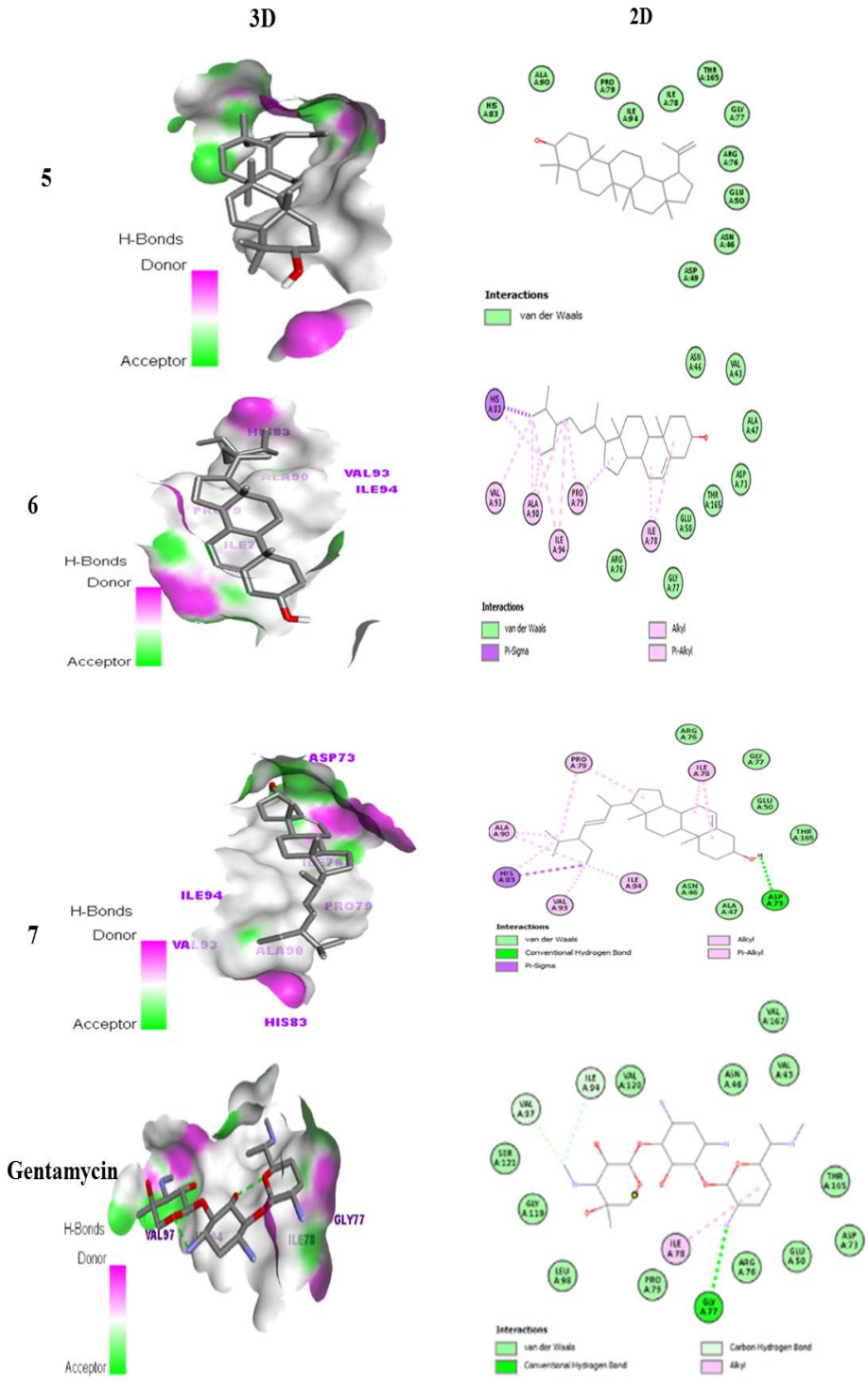

Figure 3. *The 3D and 2D modes of interactions of isolated compounds and gentamycin against E. coli DNA. gyrase B (PDB ID: 7P2M)*

The docking study with *S. aureus* pyruvate revealed that the compounds 1–7 had binding affinities ranging from -6.4 to -11.1 kcal/mol in comparison to the binding affinity of the common medication, Gentamycin, at -6.9 kcal/mol. Compound **1** had the greatest docking score (-11.1 kcal/mol), while compound **5** had the lowest (-6.4 kcal/mol). All the isolated compounds had higher binding affinity than gentamycin except compounds **5** and **6**. All compounds except compound **7** showed H-bonding interaction. The isolated compounds except compound **5** showed hydrophobic and electrostatic interactions with the protein *S. aureus* pyruvate kinase, as shown in Table 5 and Figure 4.

Table 5.

Gentamycin and isolated compounds molecular docking results against S. aureus pyruvate kinase.

Ligand	Binding affinity (kcal/mol)	H-bonding	Hydrophobic and Electrostatic	Van der Waals
1	-11.1	Asn-369,369, Thr-366, Ser-362	Pi-Cation:His365,Pi-Sigma:His365,Ile-361,361	Leu-370,Thr-353,353,366,Ser-354,362,Ala-358
2	-9.2	Ser-362,362, Thr-366	Pi-Cation:His-365,365 Pi-Sigma:Ile-361	Thr-353,Asn-369,Ala-358
3	-9.4	Ser-362,Thr-366,Ser-362	Pi-Cation: His-365,365, Pi-Sigma-Ile-361, Pi-	Asn-369,Thr-353,Asn-369,Ala-358
4	-9.3	Thr-366,His-365	Pi-Cation : His-365, Pi-Sigma: Ile-361,	Thr-348, Thr-353,Asn-369, Ala-358,Thr-366,Ser-
5	-6.4	Ser-345	-	His-365,365,Lys-341,Asn-369,Thr-348,353,Ile-361,
6	-6.6	Thr-366	Akyl and Pi-Akyl: His-365,Ile-361	Ser-345,Leu-344,Leu-368,Thr-348,Lys-341,Asn-369,Ala-358,Met-467,Ser-362, 362
7	-7.1	-	Pi-Sigma:His-365, Akyl and Pi-Akyl: Ile-361,361	Ser-362, 362,Thr-366,Thr-353, 353,His-365,Ala-358,Asn-369,369, Thr-348,348
Gentamycin	-6.9	Lys-341,His365, Ser362,362,His-365	Ser-345,Asn-369,Ther-353,366,348,Ala-358,Ile-361	Ser-362,362,His-365

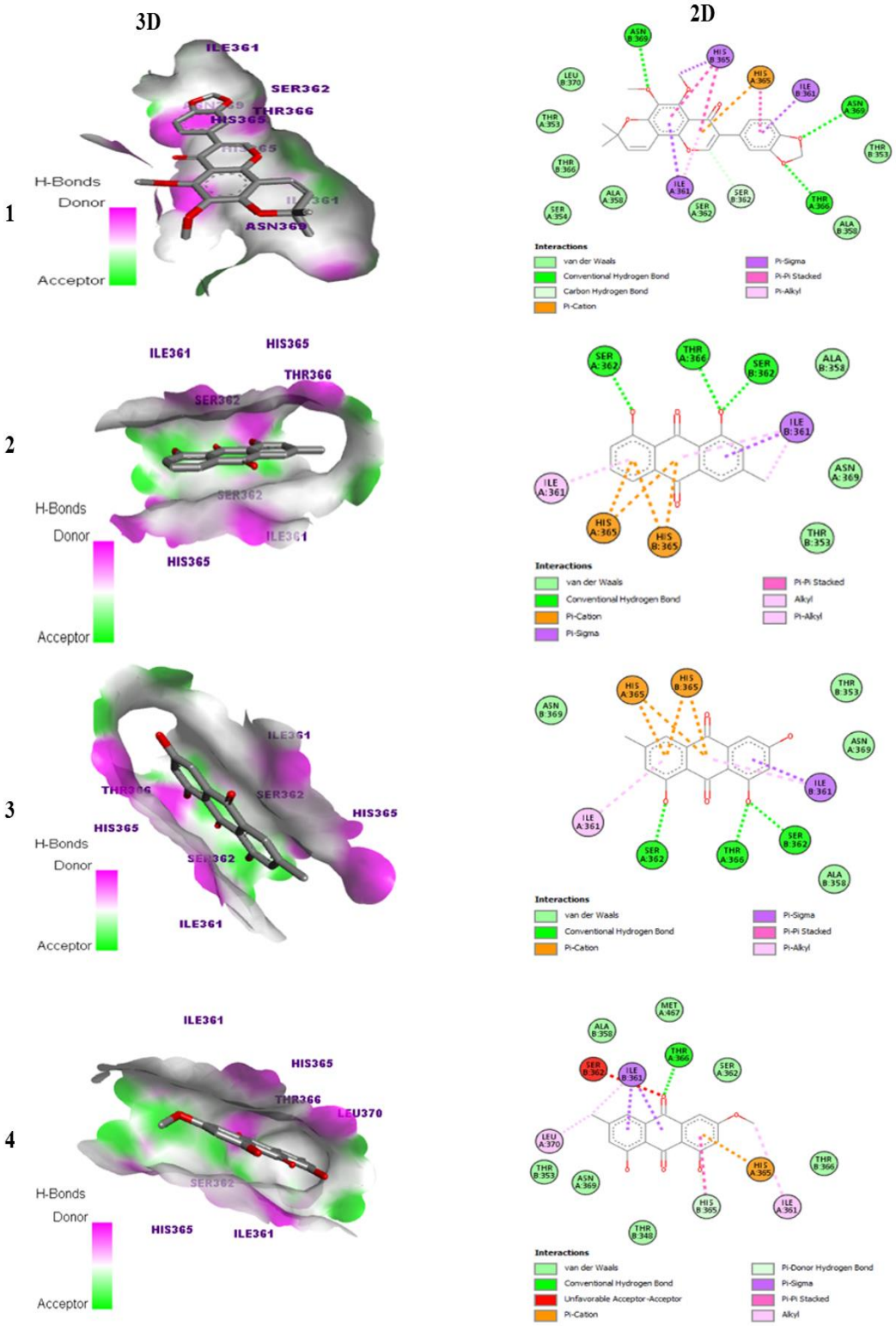
3D
2D
1
ILE361
SER362
THR366
HIS365
ASN369
H-Bonds
Donor
Acceptor
Interactions
van der Waals
Conventional Hydrogen Bond
Carbon Hydrogen Bond
Pi-Cation
Pi-Sigma
Pi-Pi Stacked
Pi-Alkyl
2
ILE361
HIS365
THR366
SER362
H-Bonds
Donor
Acceptor
Interactions
van der Waals
Conventional Hydrogen Bond
Pi-Cation
Pi-Sigma
Pi-Pi Stacked
Alkyl
Pi-Alkyl
3
ILE361
THR366
SER362
HIS365
H-Bonds
Donor
Acceptor
Interactions
van der Waals
Conventional Hydrogen Bond
Pi-Cation
Pi-Sigma
Pi-Pi Stacked
Pi-Alkyl
4
ILE361
HIS365
THR366
LEU370
SER362
H-Bonds
Donor
Acceptor
Interactions
van der Waals
Conventional Hydrogen Bond
Unfavorable Acceptor-Acceptor
Pi-Cation
Pi-Donor Hydrogen Bond
Pi-Sigma
Pi-Pi Stacked
Alkyl

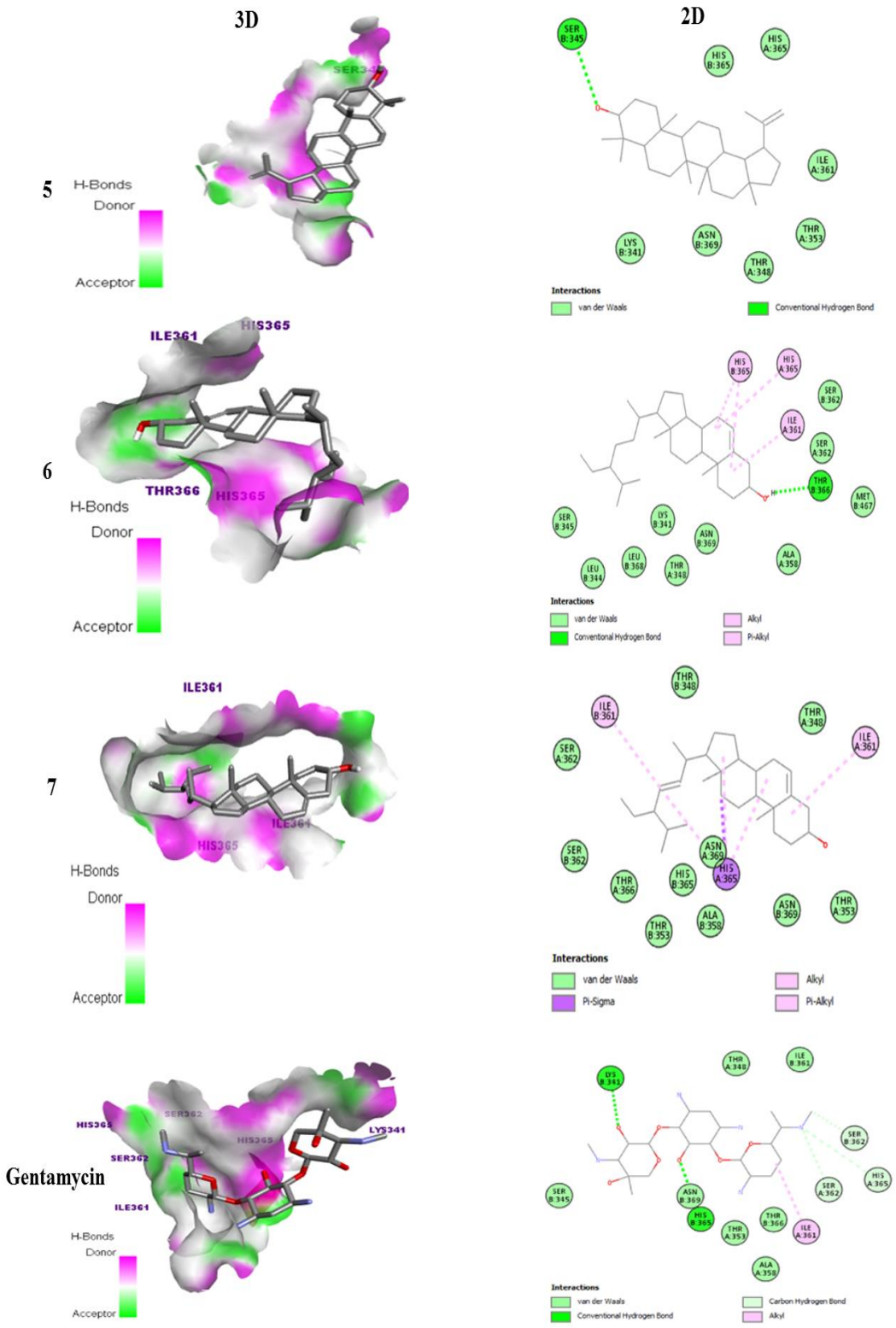

Figure 4 *The 3D and 2D modes of interactions of isolated compounds and gentamycin against S.aureus pyruvate kinase (PDB ID: 3TO7)*

Analysis of the Isolated Compounds' Toxicity and In-Silico Pharmacokinetics

The principles of Lipinski's rule evaluate the in-silico drug-likeness of the isolated compounds **1**–**7** (Lipinski et al., 2012). and Veber's rule (Veber et al., 2002) (Table 6). Compounds **1–4** do not contradict Lipinski's and Veber's rules, which means they have a good potential to be considered as drug candidates. It is indicated that they can be delivered orally as a medication rather than conventional gentamycin. Compounds **5–7** contain one violation of Lipinski's and Veber's rules, suggesting minimum lipophilicity represented by Log P (MLOGP > 5), as seen in Table **6.** ProTox-3.0 Utilizing internet resources, determine the toxicity profile of the isolated chemicals. The investigated isolated compounds showed LD50 (mg/kg) values ranging from 890 to 5000, suggesting that they would be toxic if consumed (300 LD50 ≤ 5000). (Lipinski et al., 2012). Compounds **1, 2**, **3**, and **4** showed projected toxicity class 5, indicating that they did not affect organic toxicity, implying that they might be developed as a medication candidate. Compounds **6** and **7** predicted immunotoxicity and BBB-barrier, compounds **2** and **4** predicted immunotoxicity and mutagenicity, compound **3** is active only in mutagenicity, compound **5** can affect BBB-barrier and nutritional toxicity, and compound **1** can predict immunotoxicity and ecotoxicity, as shown in Table 6.

Table 6

*Insilico Drug-likeness and Toxicity Predictions of compounds **1-7** and Gentamycin using SwissADME,and the Pro Tox 3.0 online tool*

Predicted Parameters		Ligand							
		1	2	3	4	5	6	7	Gentamycin
Drug-likeness	MF	$C_{23}H_{20}O_7$	$C_{15}H_{10}O_4$	$C_{15}H_{10}O_5$	$C_{16}H_{12}O_5$	$C_{30}H_{50}O$	$C_{29}H_{50}O$	$C_{29}H_{48}O$	$C_{21}H_{43}N_5O_7$
	MW/g/mol	408.4	254.2	270.4	284.3	426.7	414.7	412.7	477.6
	NRB	3	0	0	1	1	6	5	7
	NHA	7	4	5	5	1	1	1	12
	NHD	0	2	3	2	1	1	1	8
	TPSA (A^{o2})	76.4	74.6	94.8	93.8	20.2	20.2	20.2	199.7
	LogP (MLOGP≤4.15)	4.28	2.18	1.89	2.19	6.92	6.73	6.62	-3.33
	Log S/ESOL	-5.00	-4.11	-3.67	-3.87	-8.6	-7.9	-7.5	0.24
	Lipinski's rule of 5 violated	0	0	0	0	0	1	1	2
Toxicity Prediction	LD_{50}(mg/Kg)	3850	5000	5000	5000	2000	890	890	5000
	Toxicity class	5	5	5	5	4	4	4	5
	Organ toxicity predicted	-	-	-	-	respi	respi	respi	Nephron and respi
	Toxicological endpoints predicted	immuno and Ecotoxicity	immuno and mutagenicity	Mutagenicity	immuno and mutageniciy	BBB-barrier and nutri	immuno and BBB-barrier	immuno and BBB-barrier	immuno

CONCLUSION

In this investigation, seven compounds were recognized from the roots of *Stephania abyssinica*. This is the first report from this plant species. The crude extracts and the isolated compounds have shown antibacterial activity against the tested bacterial strains, with the crude extract showing maximum growth inhibition against *S. aureus* and *E. coli*. Compounds **2** and **6** had better infection zones against *P. aeruginosa*. The *in silico* molecular docking analysis was also used to validate the in *vitro* antibacterial activities of the isolated compounds. The molecular docking analysis showed that the isolated compounds, except for compounds **6** and **5**, have better binding affinity than the standard antibacterial drug Gentamycin. Furthermore, compounds **1-4** showed the highest drug-likeness characteristics, indicating that these compounds have remarkable biological activities and the potential to function as drugs. The traditional uses of *Stephania abyssinica* roots are supported by experimental studies that indicate the potential use of the plant for bacterial treatment. . More thorough assessments are advised to reach a definitive conclusion about the formulation potential of the plant and its medicinal uses, including in *vivo* antibacterial activity testing.

CRediT authorship contribution statement

Diriba Borena: Conceptualization, Writing – original draft **Zelalem Abdissa:** Investigation, Data curation **Girmaye Kenasa:** Methodology, Visualization **Fekadu Gurmessa:** Validation, Resources **Tolessa Duguma:** Software **Desalegn Abebe:** Formal analysis **Negera Abdissa:** Writing - Review & Editing, Supervision

Declaration of competing interest

The authors declare that there is no conflict of interest.

Data availability

Data will be made available on request

Acknowledgment

The authors would like to sincerely thank Professor Sileshi Nemomissa of the Biology Department at Addis Ababa University for identifying the plant material. Diriba Borena also thanks the Oromia Regional Educational Bureau and Horro Guduru Wallaga Zone, Shambu Preparatory School, for their scholarship support in pursuing my PhD. Finally, I extend my appreciation to Wallaga University for their financial support and for allowing me to pursue my PhD.

REFERENCES

Abebe, W. (2016). An Overview of Ethiopian Traditional Medicinal Plants Used for Cancer Treatment. *European Journal of Medicinal Plants*, *14*(4), 1–16. https://doi.org/10.9734/ejmp/2016/25670

Alex, A. A., Uba, A., Birnin-Yauri, U. A., & Yusuf, A. J. (2024). Isolation and Characterization of Antimicrobial Constituent(s) from the Stem of Cissus populnea Guill. & Perr. *Drugs and Drug Candidates*, *3*(1), 172–183. https://doi.org/10. 3390/ddc3010010

Ayele, T. T., Gurmessa, G. T., Abdissa, Z., Kenasa, G., & Abdissa, N. (2022). Oleanane and Stigmasterol-Type Triterpenoid Derivatives from the Stem Bark of Albizia gummifera and Their Antibacterial Activities.

Journal of Chemistry, 2022. https://doi.org /10.1155/202 2/9003143

Birhanu, Z., Endale, A., & Shewamene, Z. (2015). An ethnomedicinal investigation of plants used by traditional healers of Gondar town, North-Western Ethiopia. *Article in Journal of Medicinal Plants Studies*, *3*(2), 36–43. https://www.researchgate.net/publication/ 276352858

Daina, A., Michielin, O., & Zoete, V. (2017). SwissADME: A free web tool to evaluate pharmacokinetics, drug-likeness and medicinal chemistry friendliness of small molecules. *Scientific Reports*, *7*(January), 1–13. https://doi.org/10.1038/srep42717

Duval, J., Pecher, V., Poujol, M., & Lesellier, E. (2016). Research advances for the extraction, analysis and uses of anthraquinones: A review. *Industrial Crops and Products*, *94*, 812-833. https://doi.org/10.1016/j.indcrop .201 6.09.056

Degfie, T., Endale, M., Tafese, T., Dekebo, A., & Shenkute, K. (2022). In vitro antibacterial, antioxidant activities, molecular docking, and ADMET analysis of phytochemicals from roots of Hydnora johannis. *Applied Biological Chemistry*, *65*(1). https://doi.org/10.1186/s1 3765-022-00740-8

Endale, M., Eribo, B., Alemayehu, I., Kibret, B., & Mammo, F. (2016). Phytochemical Analysis of Roots of Aloe gilbertii and Millettia ferruginea. *Journal of Science & Development*, *4*(1), 23–30. https://www.researchgate.net/publication / 36595861

Erwin, P. W. R., Safitry, R. D., Marliana, E., Usman, & Kusuma, I. W. (2020). Isolation and characterization of stigmasterol and β-sitosterol from wood bark extract of baccaurea macrocarpa miq. Mull. arg. *Rasayan Journal of Chemistry*, *13*(4), 2552–2558http://dx.doi. org/10.31788/RJC.2020.1345652.

Firehun, B., & Nedi, T. (2023). Gastroprotective Activities of Aqueous and 80% Methanol Leaf Extracts of Stephania abyssinica (Quart.-Dill. and A. Rich.) Walp. (Menispermaceae) in Rats. *Journal of Experimental Pharmacology*, *15*, 497–512 . http://dx.doi.org/10.2147/JE P.S4 37707

Giday, M., Asfaw, Z., & Woldu, Z. (2010). Ethnomedicinal study of plants used by Sheko ethnic group of Ethiopia. *Journal of Ethnopharmacology*, *132*(1), 75–85. https://doi.org/10.1016/j.jep.2010.07.046

Giday, M., Teklehaymanot, T., Animut, A., & Mekonnen, Y. (2007). Medicinal plants of the Shinasha, Agew-awi and Amhara peoples in northwest Ethiopia. *Journal of Ethnopharmacology*, *110*(3), 516–525. https://doi.org/10.1016/j.jep.2006.10.011

Habtamu, T., & Addisu, A. (2019). In vitro antibacterial activity of Rumex nervosus and Clematis simensis plants against some bacterial human pathogens. *African Journal of Microbiology Research*, *13*(1), 14–22. https://doi.org/10.5897/ajmr2018.9017

Lipinski, C. A., Lombardo, F., Dominy, B. W., & Feeney, P. J. (2012). Experimental and computational approaches to estimate solubility and permeability in drug discovery and development settings. *Advanced Drug Delivery Reviews*, *64*(SUPPL.), 4–17. https://doi.org/10.1016/j.addr.2012.09.019

Mirutse, G., Zemede, A., & Zerihun, W. (2009). Medicinal plants of the Meinit ethnic group of Ethiopia: An ethnobotanical study. *Journal of Ethnopharmacology*, *124*(3), 513–521. https://doi.org/10.1016/j.jep.2009.05.009

Saur, I. M. L., Panstruga, R., & Schulze-Lefert, P. (2021). NOD-like receptor-mediated plant immunity: from structure to cell death. *Nature Reviews Immunology*, *21*(5), 305–318. https://doi.org/ 10.1038/s41577-020-00473-z

Shifa, M., Abdissa, D., & Asere, T. G. (2021). Chemical constituents of rumex abyssinicus roots and evaluation of its antimicrobial activities. *Journal of the Turkish Chemical Society, Section A: Chemistry*, *8*(1), 21–46. https://doi.org/10.18596/jotcsa.797560

Shwe, H. H., Win, K. K., Moe, T. T., Myint, A.

A., & Win, T. (2019). Isolation and Structural Characterization of Lupeol from the Stem Bark of Diospyros ehretioides Wall. *Ieee-Sem*, *7*(8), 140–144. http://dx.doi.org/10.4314 /jasem.v24i 6.11

Srivastava, S., Haneef, M., Saxena, V. L., Khan, M., & Khan, S. (2024). Structure and Ligand-based In Silico Studies towards the Natural Inhibitors against Receptor Recognition Spike Protein of SARS-CoV-2. *The Open Bioinformatics Journal*, *17*(1), 1–15. https://doi.org/10.2174/0118750362284177240304055831

Suleman, S., & Alemu, T. (2012). A survey on utilization of ethnomedicinal plants in Nekemte town, East Wellega (Oromia), Ethiopia. *Journal of Herbs, Spices and Medicinal Plants*, *18*(1), 34–57. https:// doi.org/10.1080/104964 75.2011.645188

Tadesse, A. A., Muhammed, B. L., & Zeleke, M. A. (2022). Chrysophanol from the Roots of Kniphofia Insignis and Evaluation of Its Antibacterial Activities. *Journal of Chemistry*, *2022*(1), 1–4. https://doi.org/10.1155/2022/ 5884309

Teklehaymanot, T., & Giday, M. (2007). Ethnobotanical study of medicinal plants used by people in Zegie Peninsula, Northwestern Ethiopia. *Journal of Ethnobiology and Ethnomedicine*, *3*, 1–11. https://doi.org/10.1186/1746-4269-3-12

Uttu, A. J., Sallau, M. S., Ibrahim, H., & Iyun, O. R. A. (2023). Isolation, characterization, and docking studies of campesterol and β-sitosterol from Strychnos innocua (Delile) root bark. *Journal of Taibah University Medical Sciences*, *18*(3), 566–578. https://doi.org/10.1016/j.jtumed.2022.12.003

Veber, D. F., Johnson, S. R., Cheng, H. Y., Smith, B. R., Ward, K. W., & Kopple, K. D. (2002). Molecular properties that influence the oral bioavailability of drug candidates. *Journal of Medicinal Chemistry*, *45*(12), 2615–2623. https://doi.org/10.1021/jm020017n

Worku, L. A., Bachheti, R. K., Bisht, S. S., Bachheti, A., & Alemu, W. K. (2024). Exploring the Medicinal Potential of Hyptis suaveolens (Lamiaceae): A Comprehensive Review of Phytochemicals, Pharmacological Properties, and Drug Development Prospects. *Natural Product Communications* , *19*(11).https://doi.org/1934578X241298919

Yiblet, T. G., Tsegaw, A., Ahmed, N., Dagnew, S. B., Tadesse, T. Y., & Kifle, Z. D. (2022). Evaluation of Wound Healing Activity of 80% Methanol Root Crude Extract and Solvent Fractions of Stephania abyssinica (Dill. & A. Rich.) Walp. (Menispermaceae) in Mice. *Journal of Experimental Pharmacology*, *14*, 255–273. https://doi.org/10.2147/jep.s364282

Zemene, M., Geta, M., Huluka, S. A., & Birru, E. M. (2021). Antimalarial Activity of the 80% Methanol Leaf Extract and Solvent Fractions of Stephania abyssinica (Dill. & A. Rich.) Walp. against Plasmodium berghei Infection in Mice. *Ethiopian Pharmaceutical Journal*, *36*(2), 109–120. https://doi.org/10.4314/epj.v36i2.4

Zeng, Y. B., Wei, D. J., Dong, W. H., Cai, C. H., Yang, D. L., Zhong, H. M., Mei, W. L., & Dai, H. F. (2017). Antimicrobial glycoalkaloids from the tubers of Stephania succifera. *Archives of Pharmacal Research*, *40*(4), 429–434. https://doi.org/10.1007/s12272-014-0467-5

Appendixes

Appendix 1:. ^{1}H NMR spectrum of (**1**) observed at 500 MHz for $CDCl_3$ solvent at 25^{0}C.

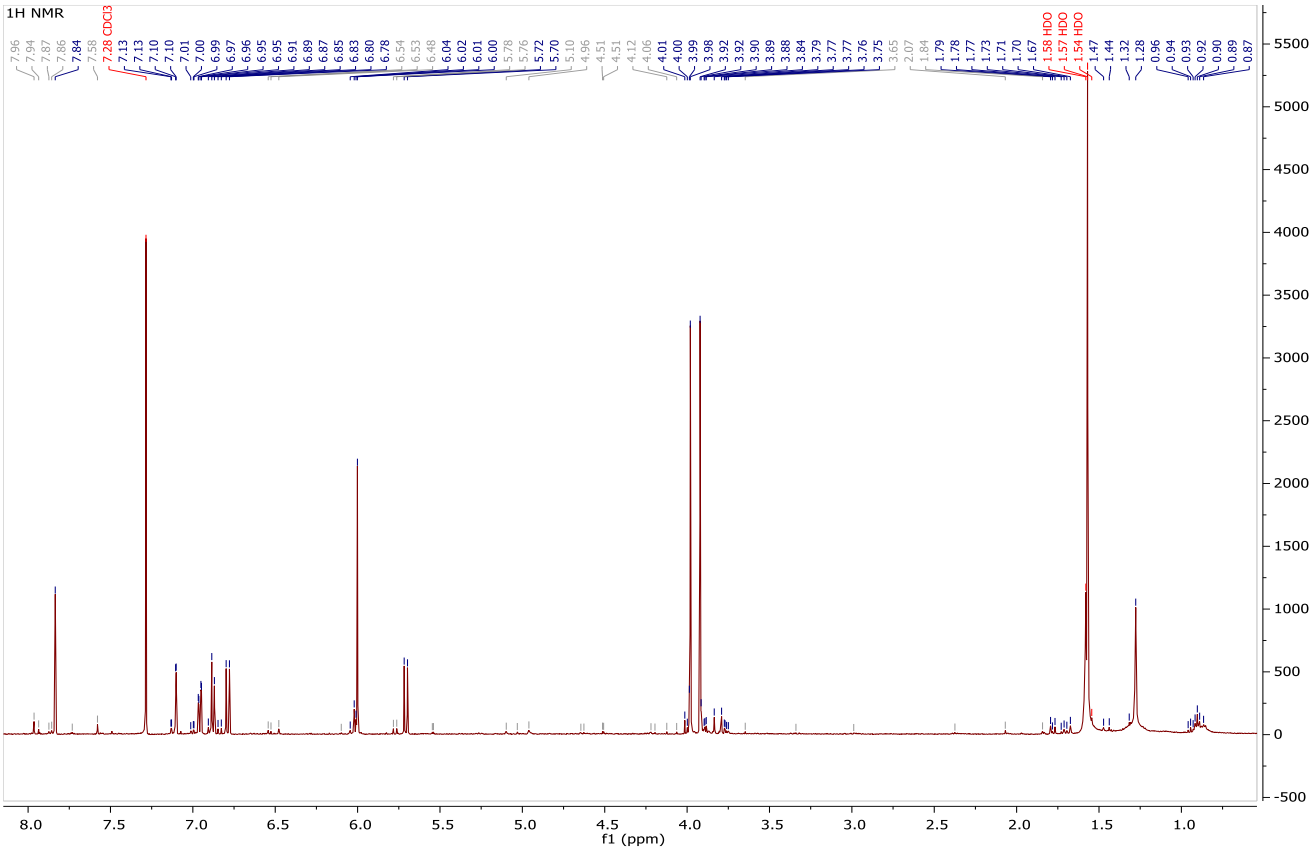

Appendix 2: ^{13}C NMR spectrum (**1**) observed at 125 MHz for $CDCl_3$ solvent at 25^0C.

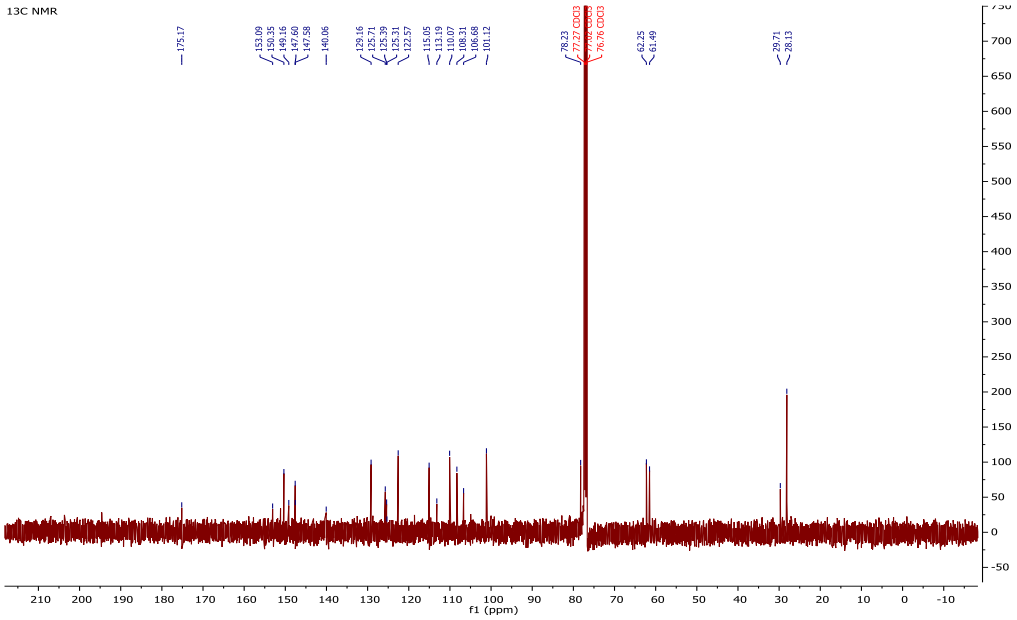

Appendix 3: 135 DEPT (**1**) observed at 125 MHz for CDCl3 solvent at 250C

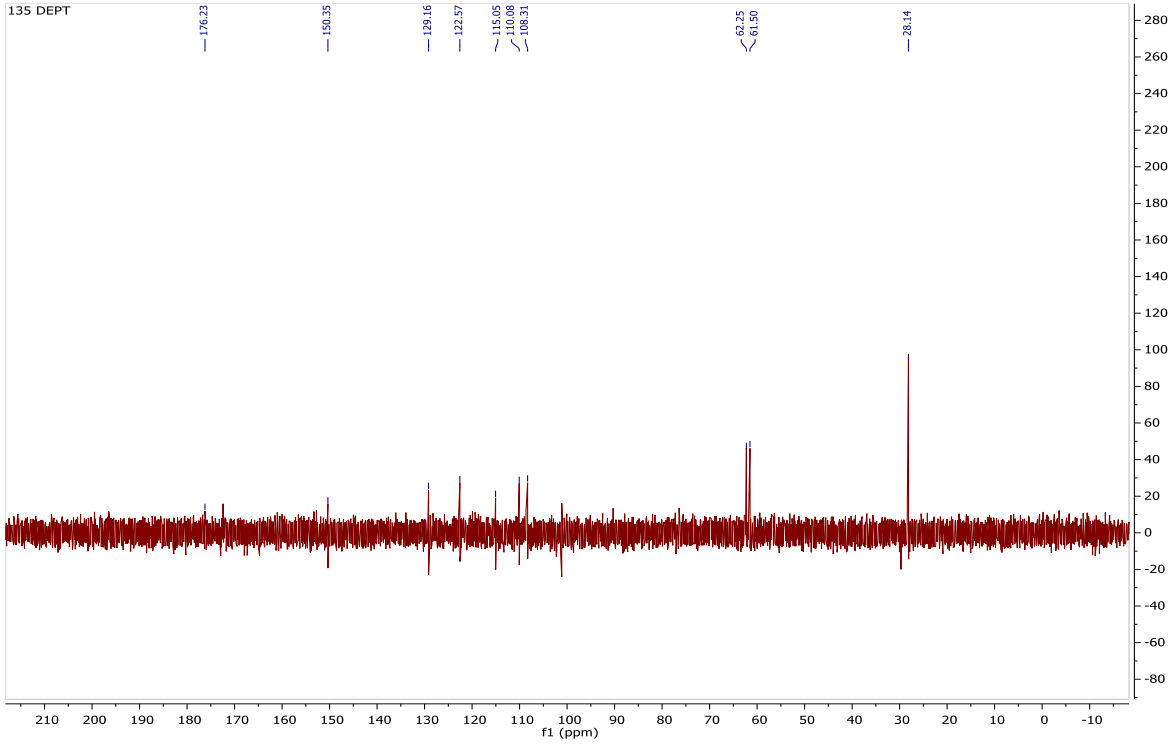

Appendix 4: COSY (**1**) observed at 500 MHz for $CDCl_3$ solvent at 25^0C

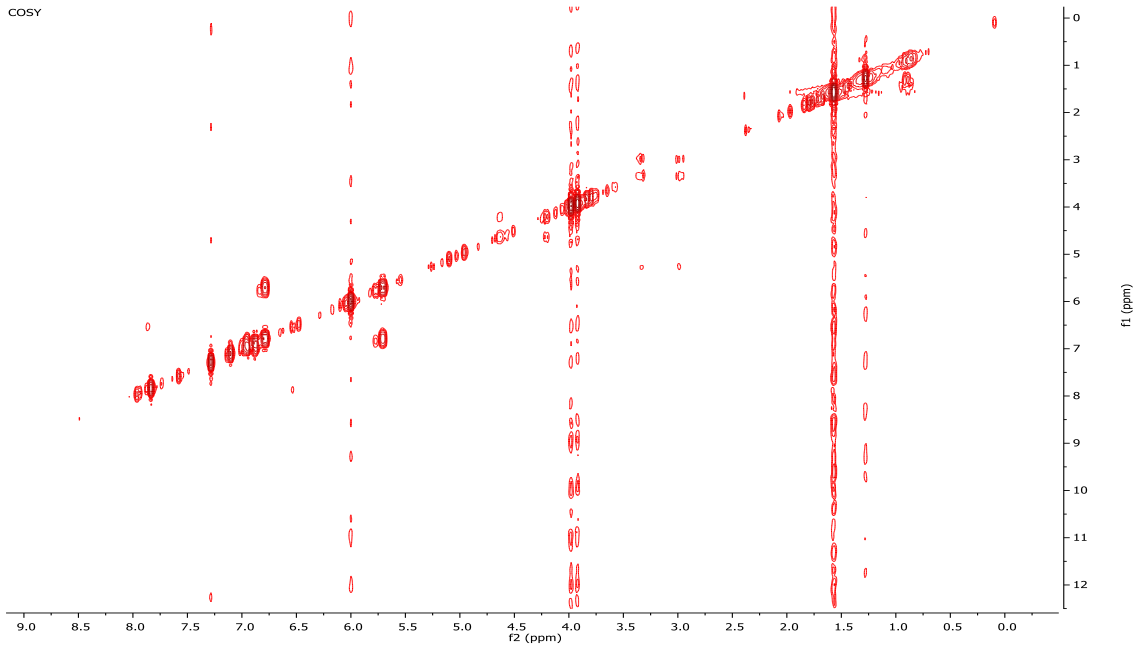

Appendix 5: HSQC spectrum of (**1**) observed at 500 MHz and 125MHz for $CDCl_3$ solvent at 25^0C**.**

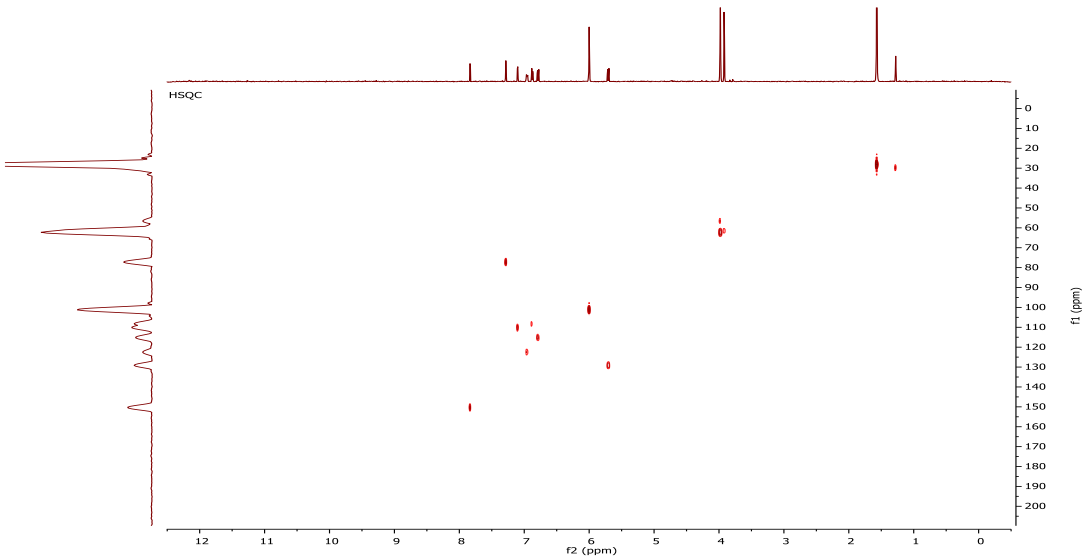

Appendix 6: HMBC spectrum of (**1**) observed at 500 MHz and 125MHz for $CDCl_3$ solvent at 25^0C

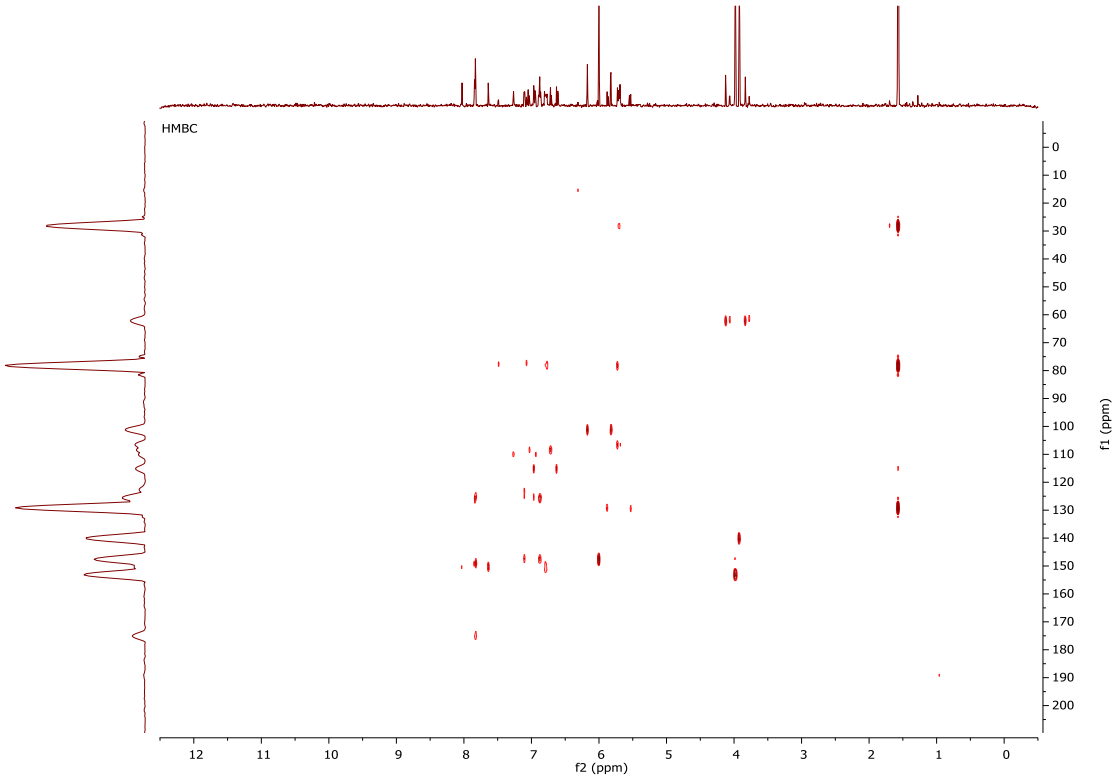

Appendix 7: The ESI-MS Spectrum of (**1**)

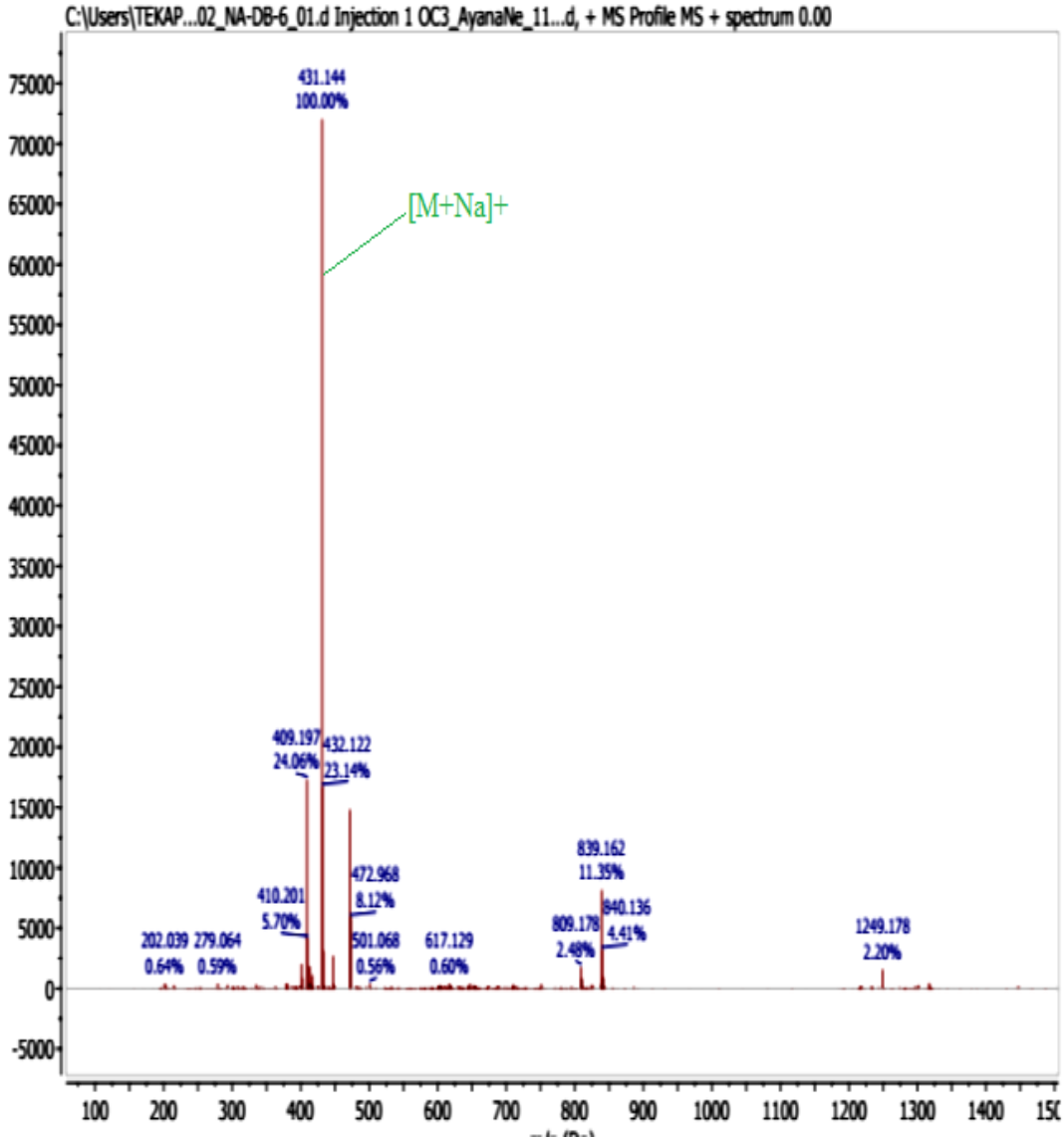

Appendix 8: ^{1}H NMR spectrum of (**2**) observed at 500 MHz for $CDCl_3$ solvent at 25^0C.

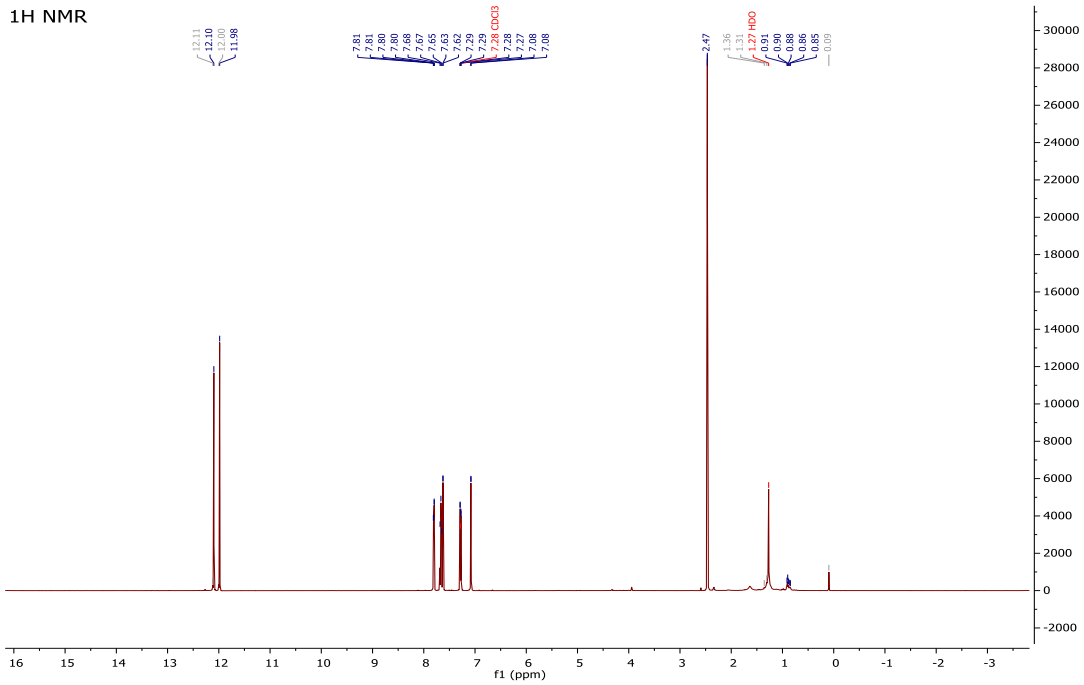

Appendix 9: ^{13}C NMR spectrum of (2) observed at 125 MHz for CDCl3) solvent at 25^0C.

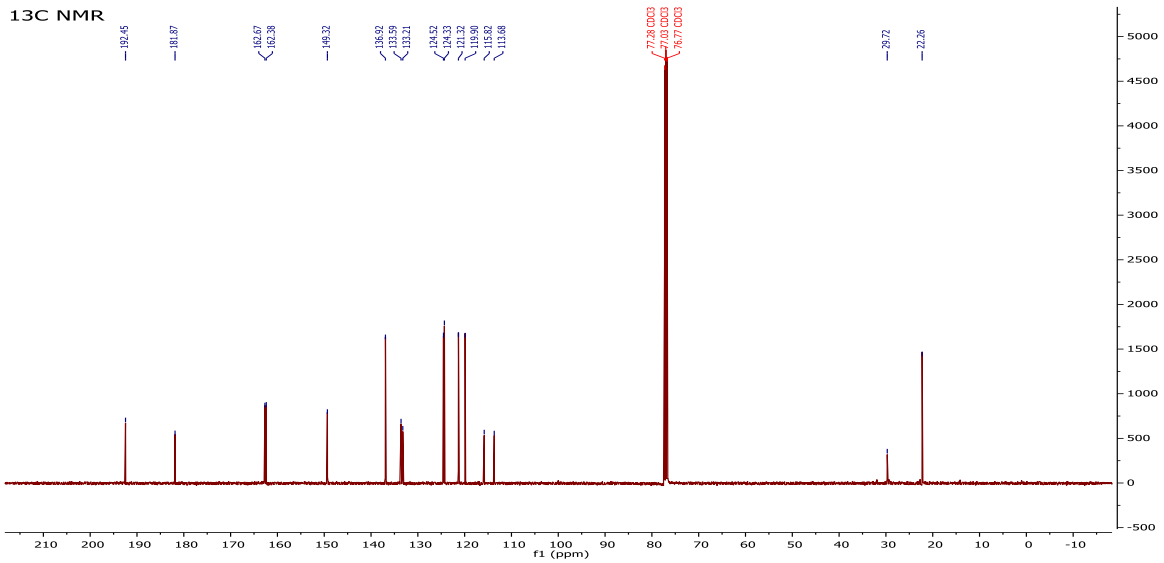

Appendix 10: ^{1}H NMR spectrum of (**3**) observed at 500 MHz for $CDCl_3$ solvent at 25^0C.

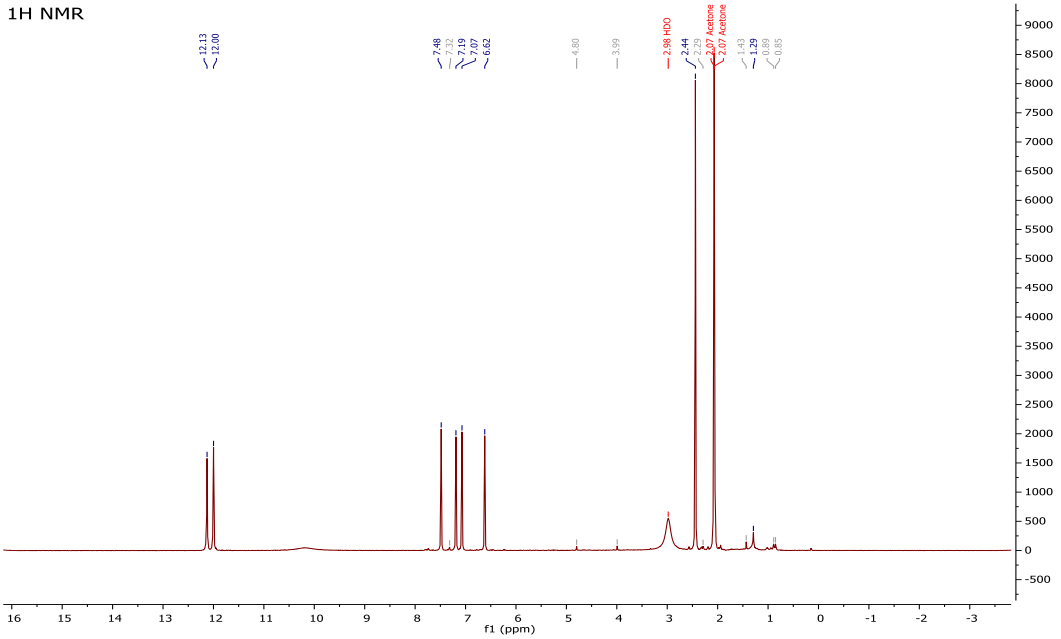

Appendix 11: ^{13}C NMR spectrum of (**3**) observed at 125 MHz, CDCl3) solvent at 25^0C

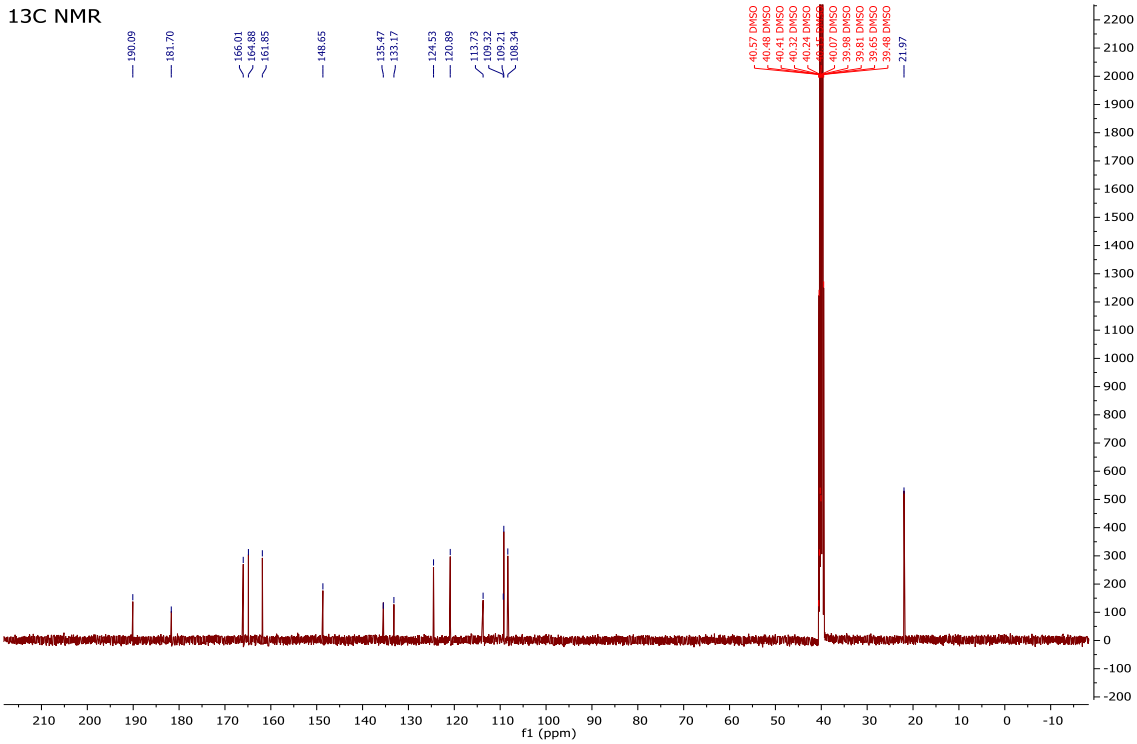

Appendix 12: COSY (**3**) observed at 500 MHz for CDCl3 solvent at 25^0C

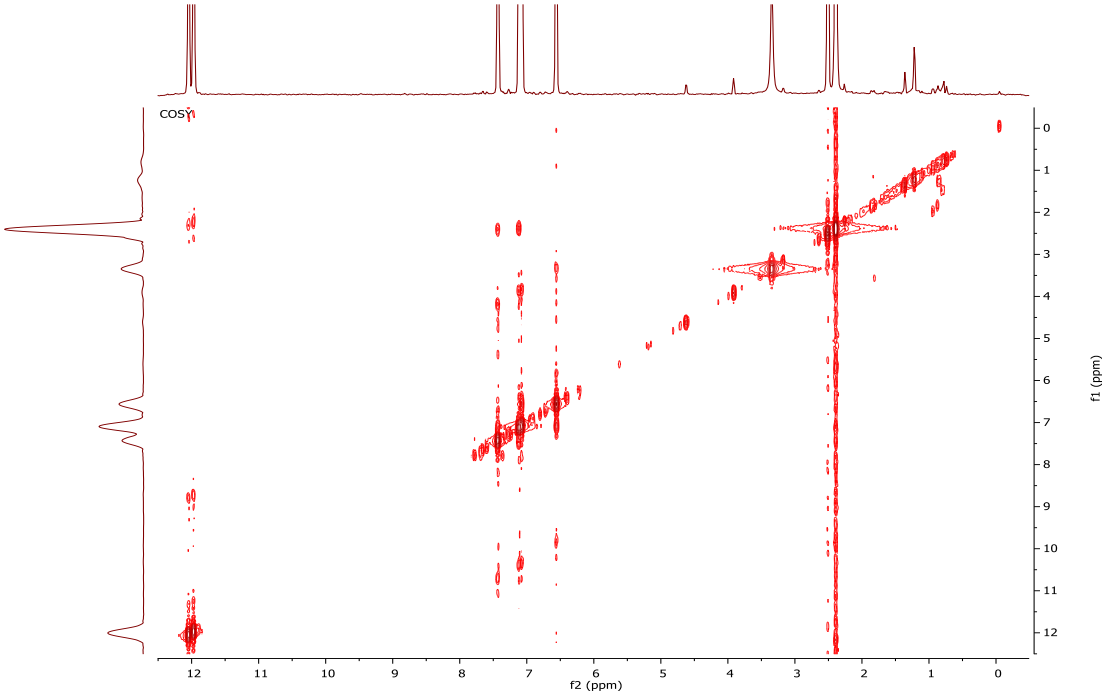

Appendix 13: HSQC spectrum of (**3**) observed at 500 MHz and 125 MHz for CDCl3 solvent at 25^0C

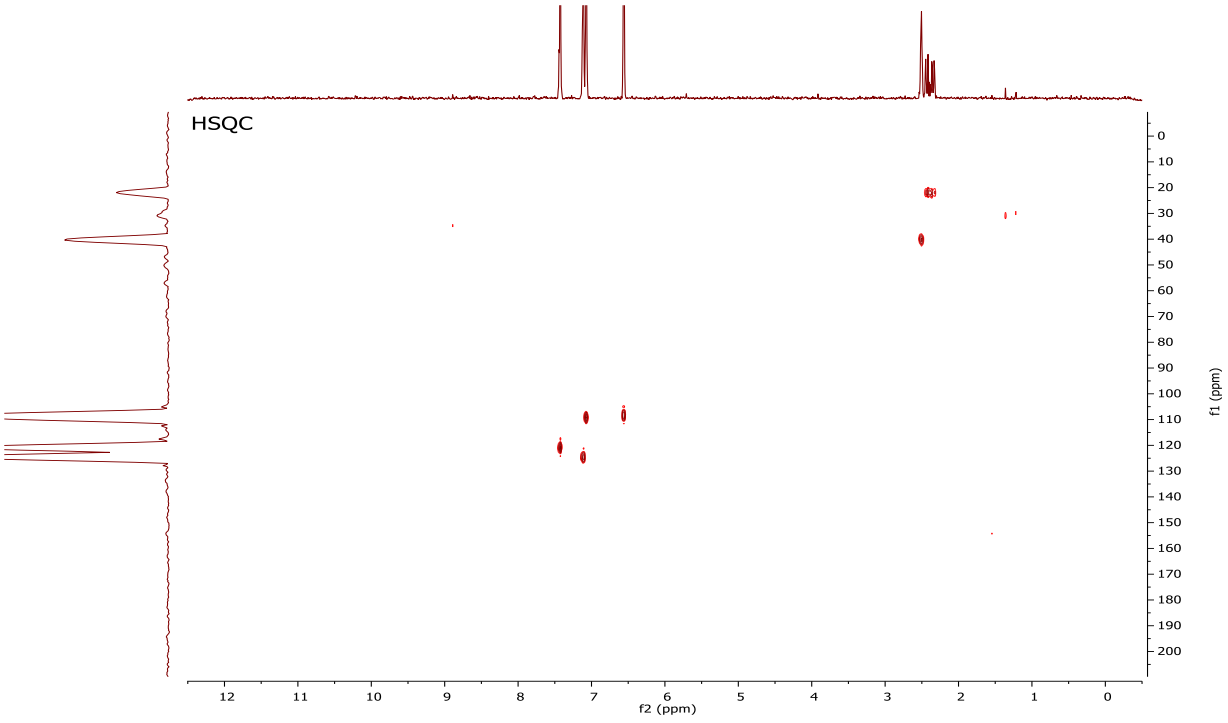

Appendix 14. HMBC spectrum of (**3**) observed at 500 MHz and 125 MHz for CDCl3 solvent at 25^0C.

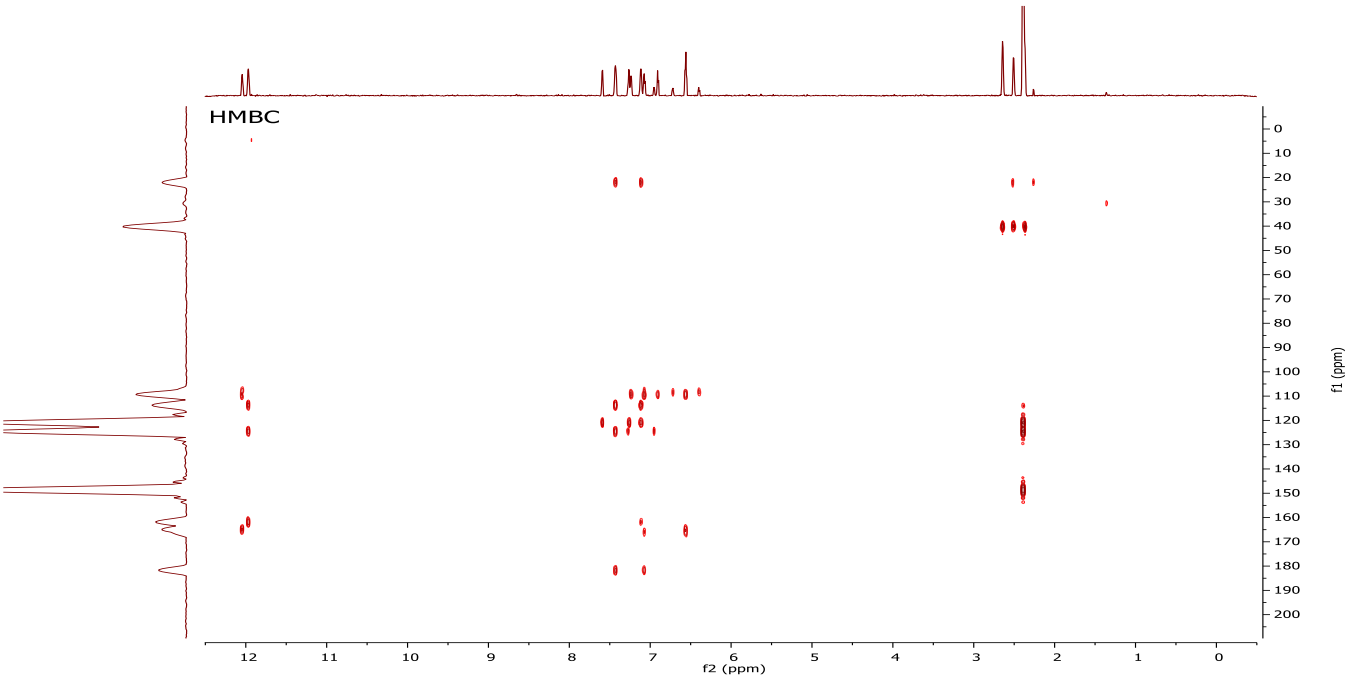

Appendix 15: 1H NMR spectrum of (**4**) observed at 500 MHz for CDCl3 solvent at 25^0C.

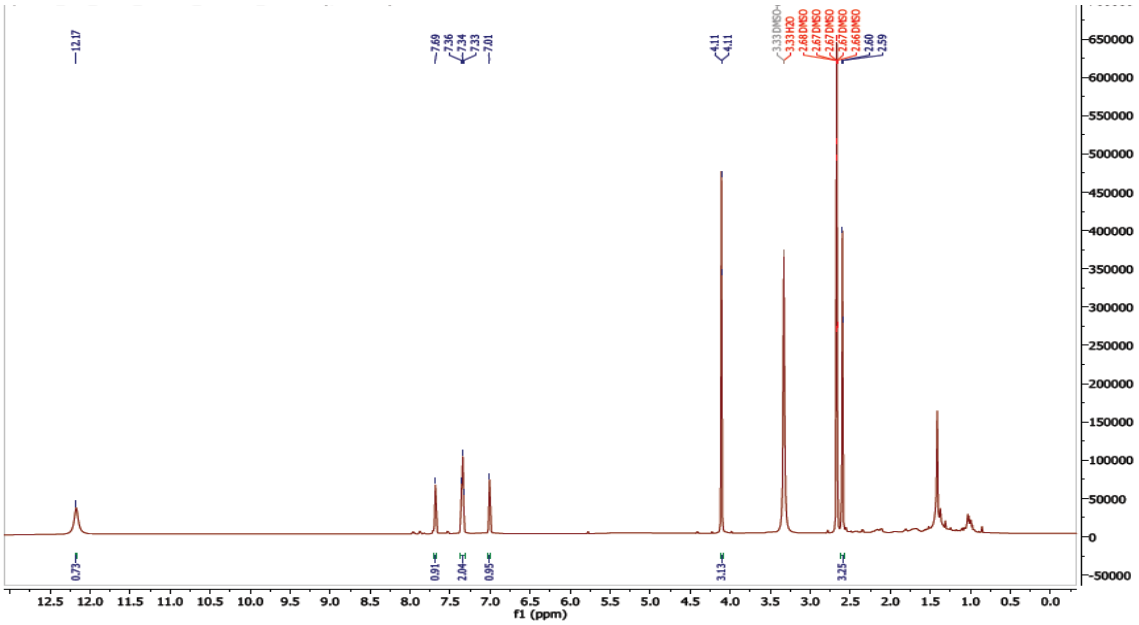

Appendix 16: 13C NMR spectrum of (**4**) observed at 125 MHz for CDCl3 solvent at 25^0C

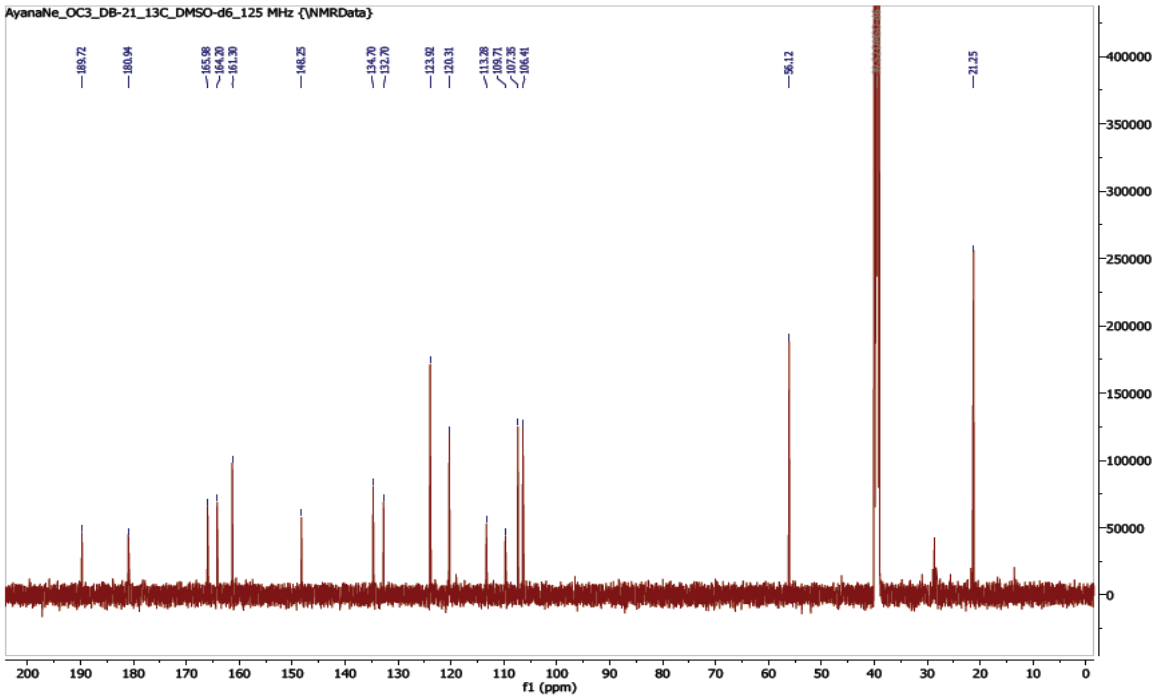

Appendix 17: COSY spectrum of (**4**) observed at 500 MHz for CDCl3 solvent at 25^0C

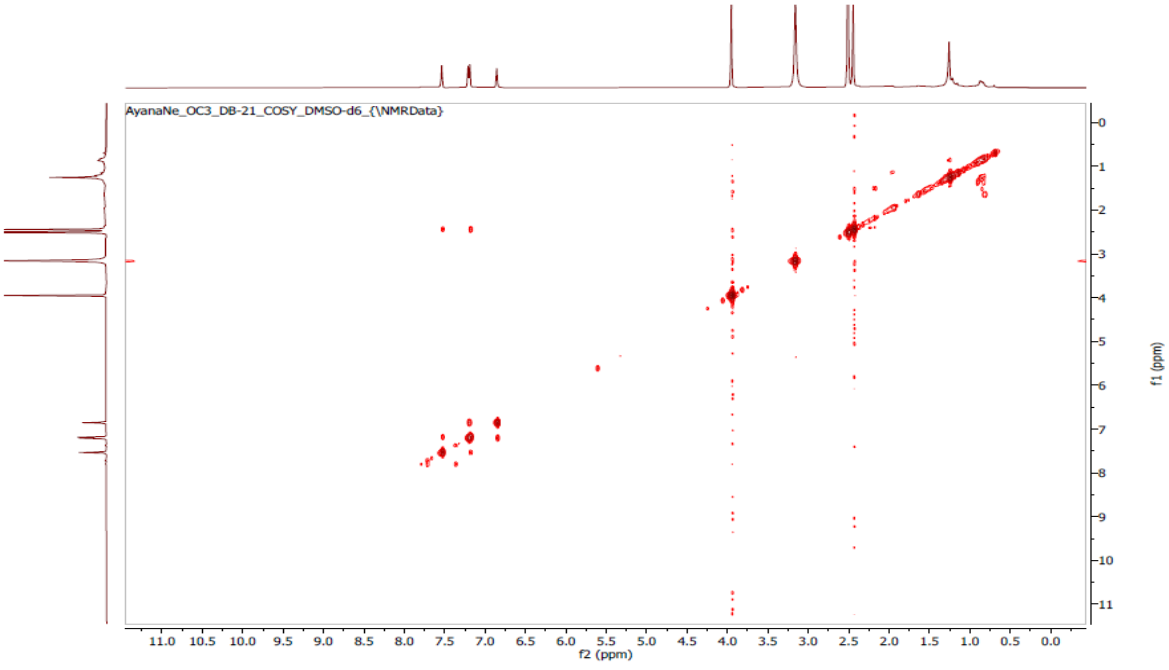

Appendix 18: HSQC spectrum of (**4**) observed at 500 MHz and 125MHz for CDCl3 solvent at 25^0C.

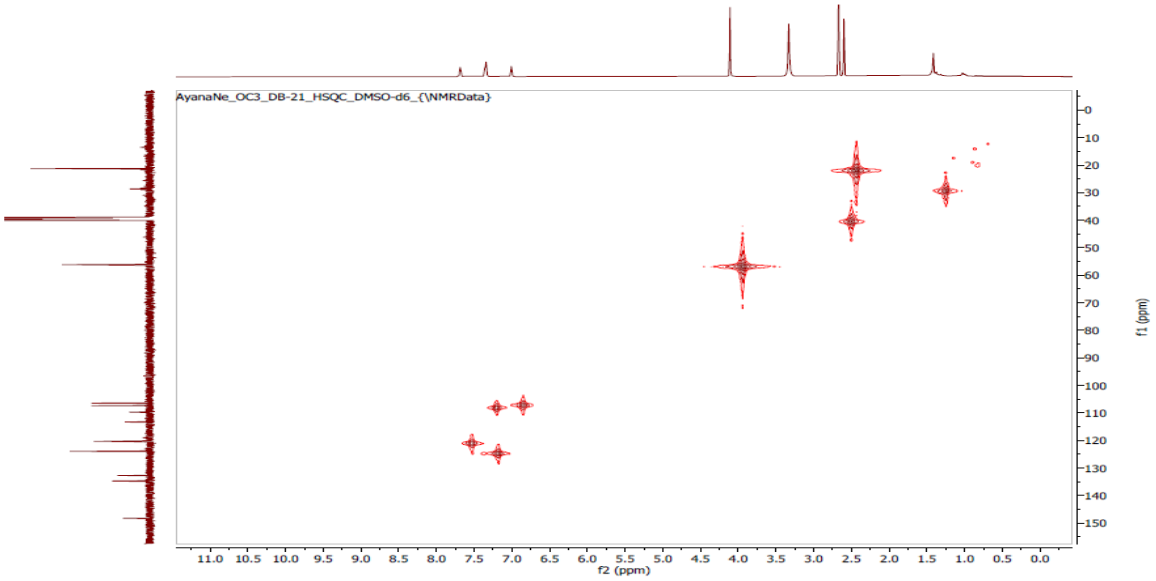

Appendix 19: HMBC spectrumof (**4**) observed at 500 MHz and 125 MHz for $CDCl_3$ solvent at 25^0C

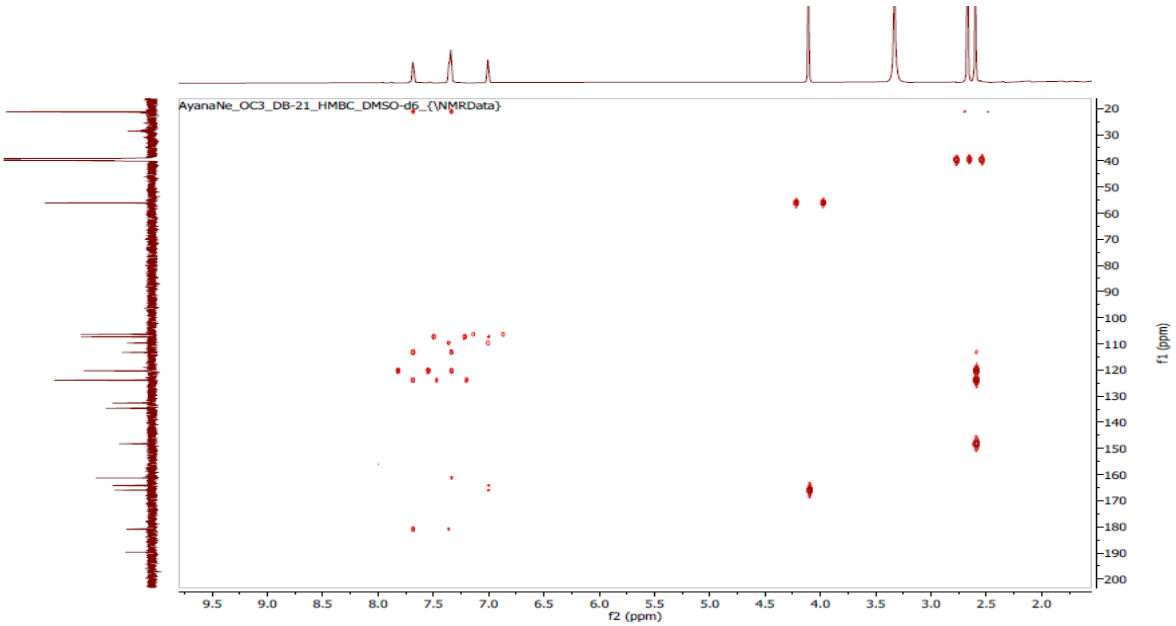

Appendix 20: ^{1}H NMR spectrum of (**5**) observed at 500 MHz for $CDCl_3$ solvent at 25^0C

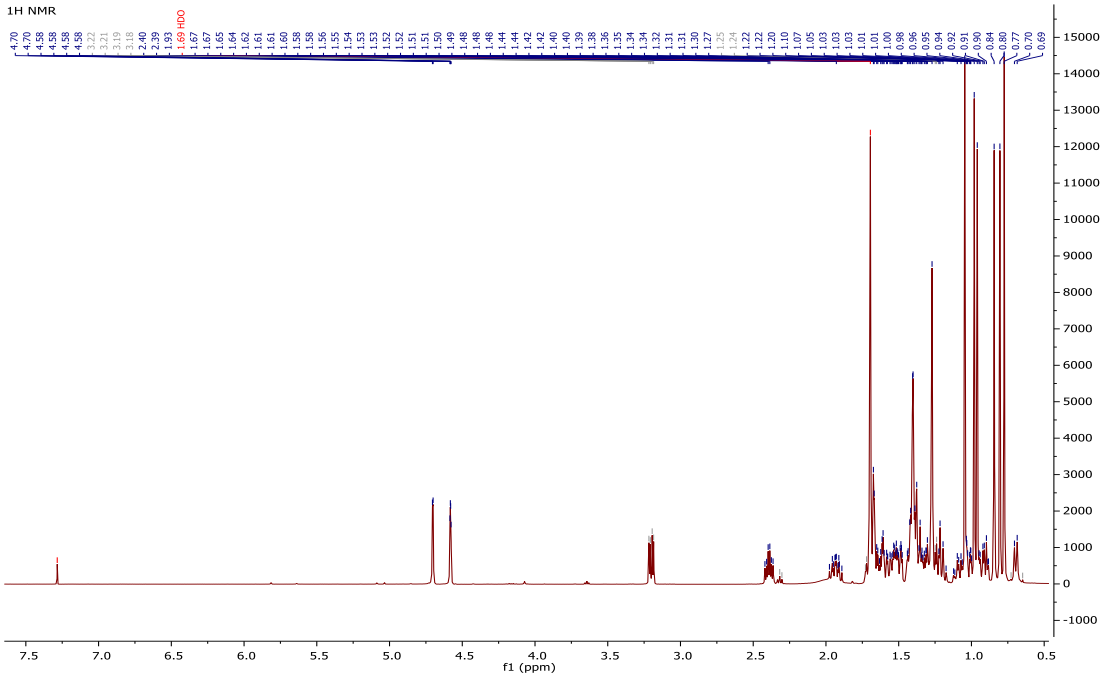

Appendix 21: ^{13}C NMR spectrum of (**5**) observed at 125 MHz for $CDCl_3$ solvent at 25^0C.

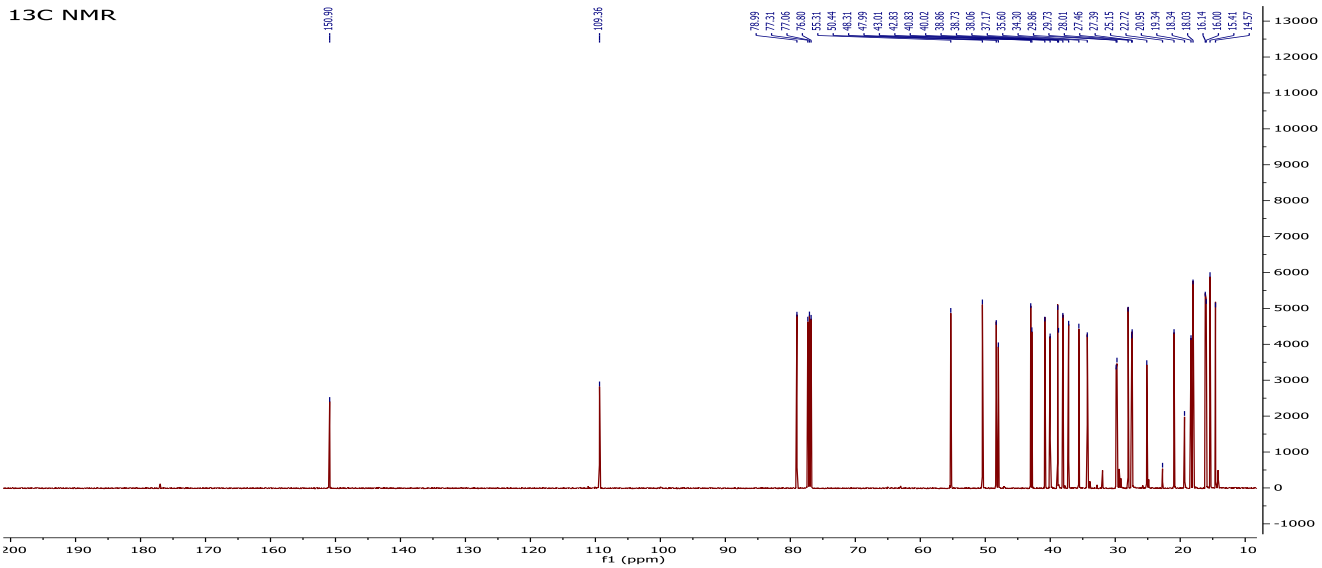

Appendix 22: COSY spectrum of (**5**) observed at 500 MHz for $CDCl_3$ solvent at 25^0C

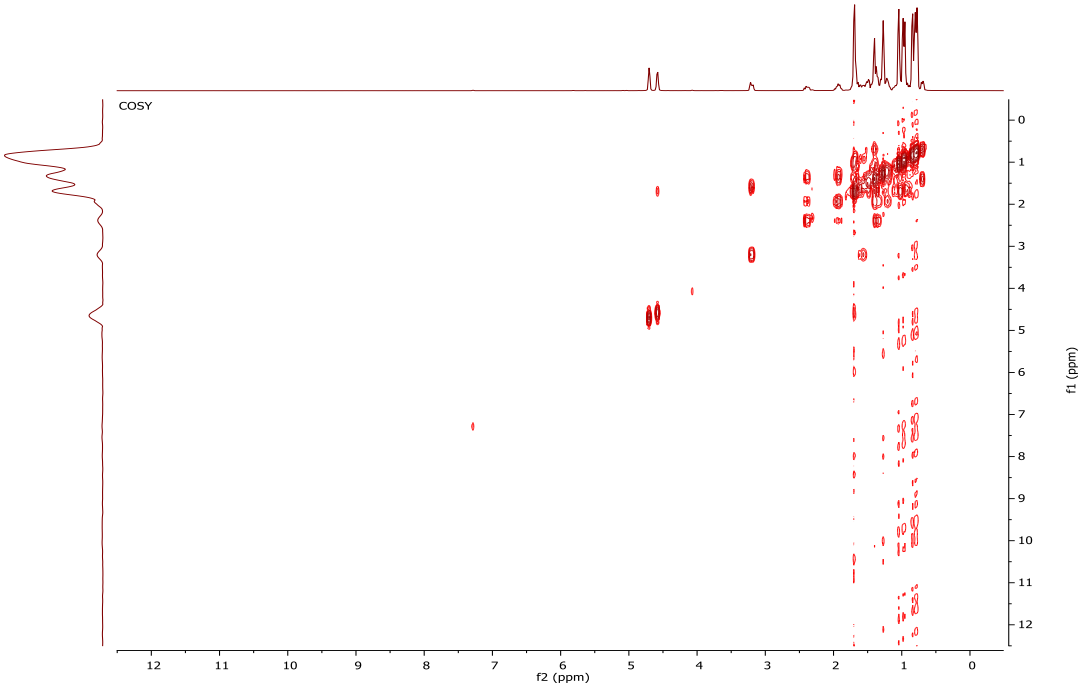

Appendix 23: HMBC spectrum of (**5**) observed at 500 MHz and 125MHz for $CDCl_3$ solvent at 25^0C

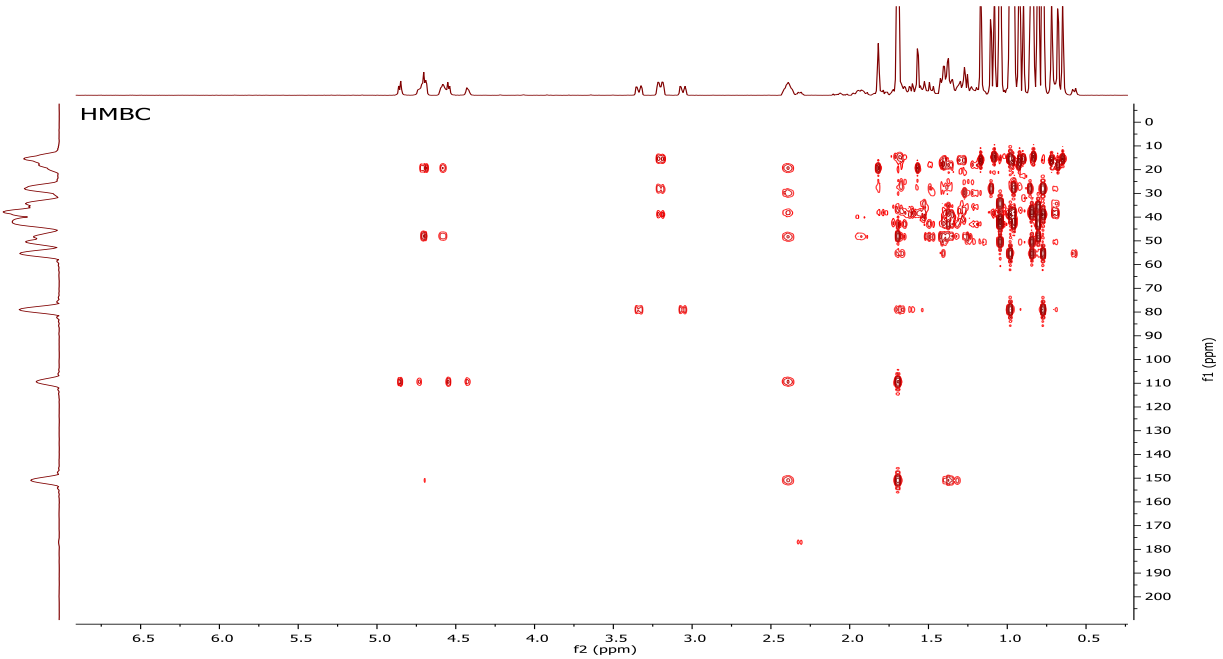

Appendix 24: ^{1}H NMR spectrum of (**6**) observed at 500 MHz for $CDCl_3$ solvent at 25^0C.

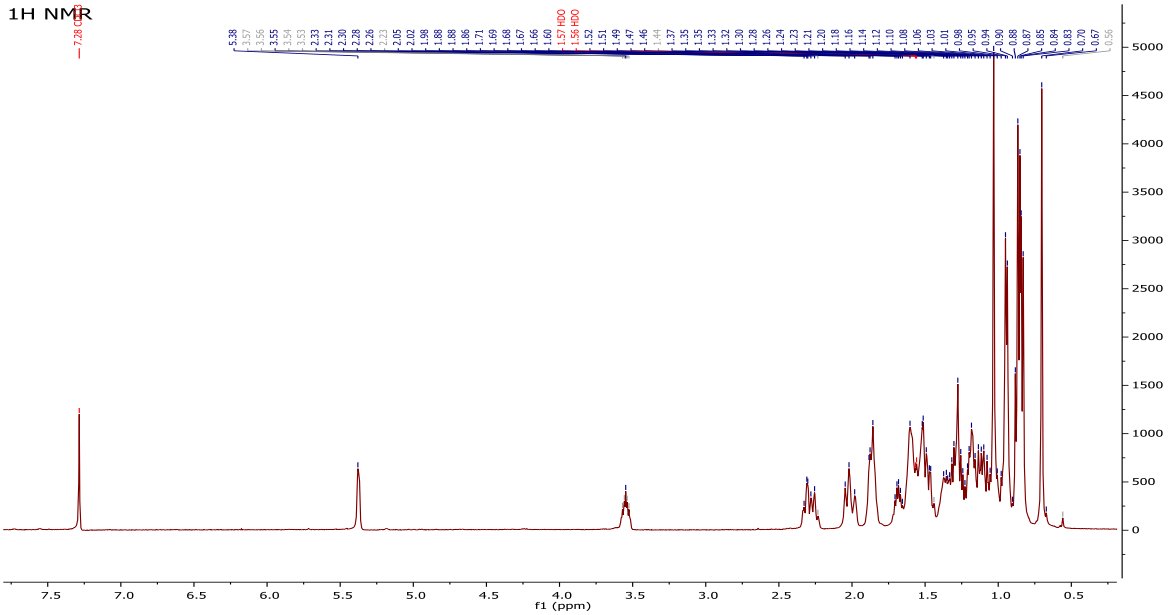

Appendix 25: ^{13}C NMR spectrum of (**6**) observed at 125 MHz for $CDCl_3$ solvent at 25^0

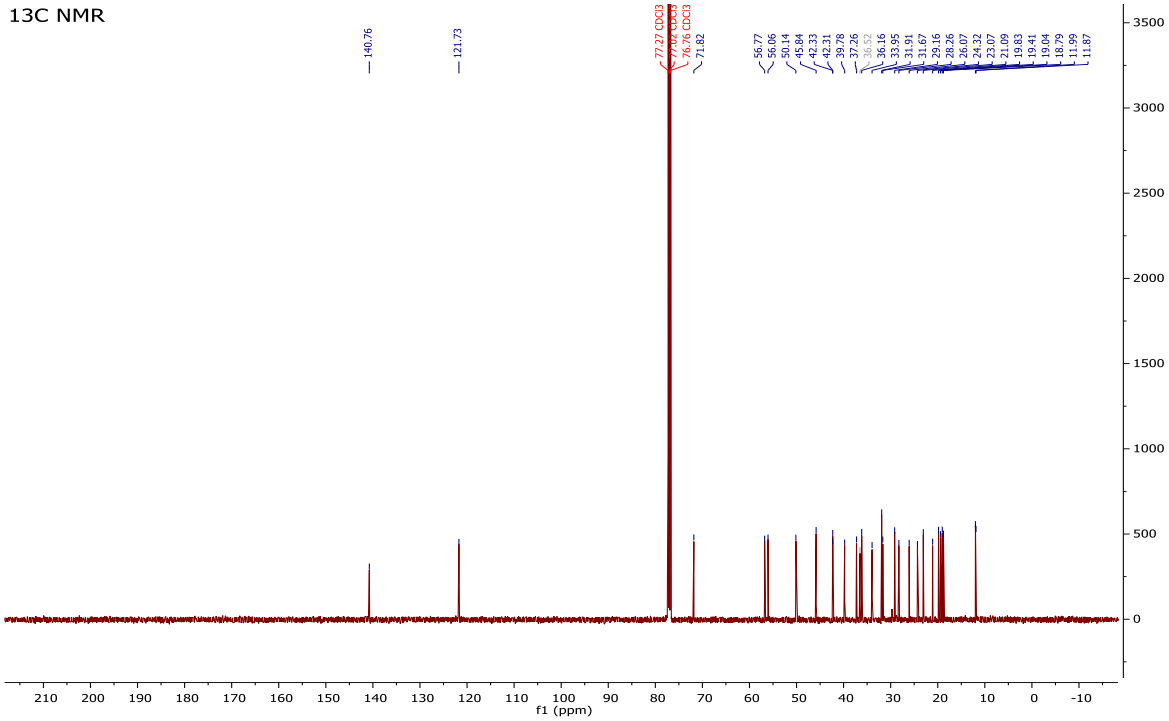

Appendix 26: ^{1}H NMR spectrum of (**7**) observed at 500 MHz for $CDCl_3$ solvent at 25^{0}C.

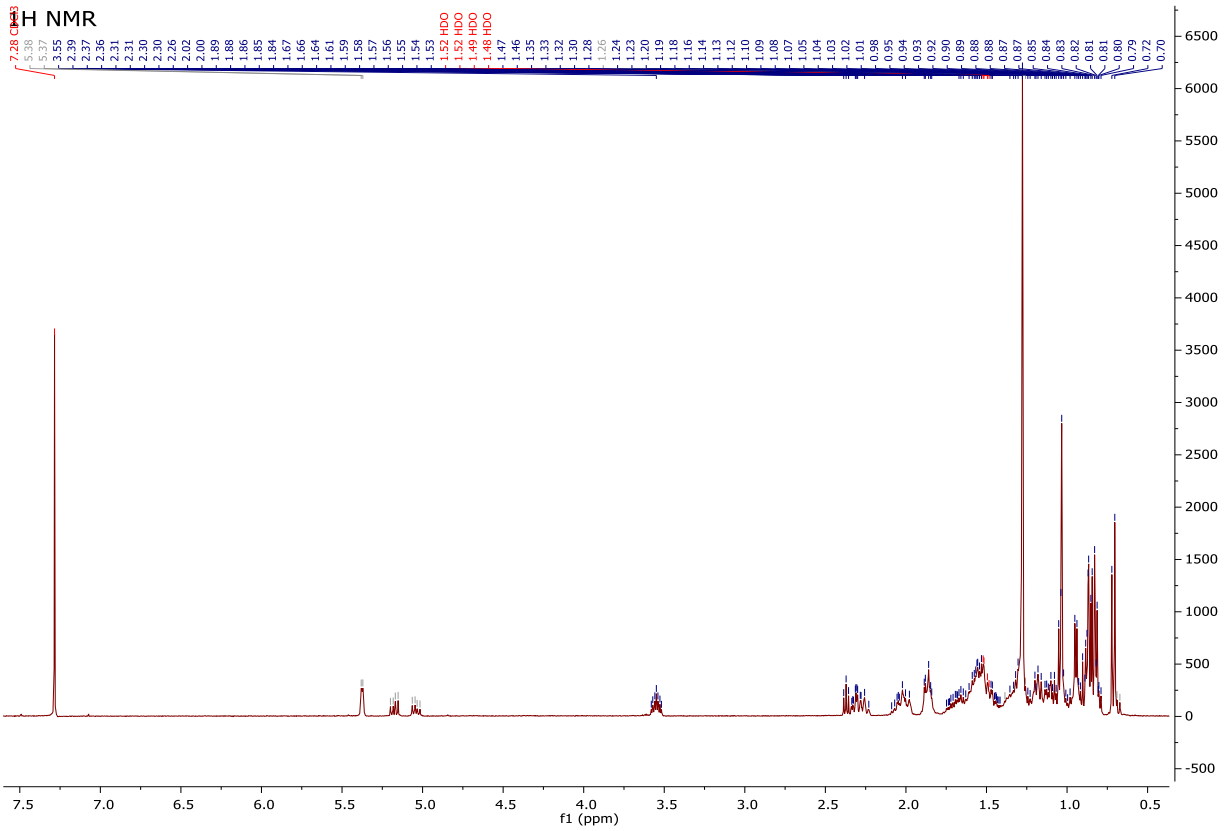

Appendix 27: ^{1}H NMR spectrum of (**7**) observed at 500 MHz for $CDCl_3$ solvent at25^{0}C.